

Simulation-Based Priors without Simulations: an Analytic Perspective on EFT Parameters of Galaxies

Mikhail M. Ivanov^{1, 2, *}

¹*Center for Theoretical Physics, Massachusetts Institute of Technology, Cambridge, MA 02139, USA*

²*The NSF AI Institute for Artificial Intelligence and Fundamental Interactions, Cambridge, MA 02139, USA*

Effective field theory (EFT)-based full-shape analysis with simulation-based priors (SBPs) is a novel approach to galaxy clustering data analysis, which significantly boosts the constraining power by efficiently incorporating field-level simulation information from small scales. So far, SBPs have been mostly extracted from a large set of mock catalogs generated with the Halo Occupation Distribution (HOD) approach. We show that given a halo mass function model and assuming that the EFT parameters of halos depend only on the peak height, HOD-based priors can be computed analytically for the standard 7-parameter HOD model. We derive the relevant expressions for deterministic EFT parameters from the halo model. The halo model, however, fails to accurately describe stochastic EFT parameters, for which we use a physically motivated phenomenological prescription. We compare our analytic priors with simulations and find an excellent agreement. Our approach provides analytic insights into the physics behind the EFT parameters of galaxies, and allows one to reduce the computation time of SBPs to virtually nothing. As an application, we produce a set of 100,000 EFT parameters by sampling both HOD and cosmological models, and explicitly demonstrate that any cosmology dependence can be completely absorbed by relatively minor shifts of the HOD parameters. Our approach can be generalized to other variants of the HOD and cosmological models beyond Λ CDM.

1. INTRODUCTION

Effective field theory (EFT) for Large-Scale Structure [1–3] is a systematic analytic approach to structure formation that provides unmatched accuracy and flexibility for quasi-linear clustering observables. It has been successfully applied to various kinds of cosmological data in the perturbative regime, e.g. galaxy clustering in redshift-space ([4–8], see also [9] for the recent application of this technique by the Dark Energy Survey Instrument collaboration), projected galaxy clustering [10], and the Lyman- α forest [11–13].

One important feature of EFT is the presence of free EFT parameters (a.k.a. “nuisance parameters”), which are not calculable within the EFT and need to be fitted from data or numerical simulations. The standard approach is to determine the EFT parameters from the data itself. While this approach produces conservative results (provided that the priors on EFT parameters are chosen to be appropriately wide), it leads to a significant degradation of constraining power, see [14, 15] for

detailed discussions.¹

In contrast, matching EFT parameters from the numerical simulations leads to a dramatic improvement of constraining power [19–21]. This approach is known as the EFT-based full-shape analysis with the simulation-based priors (SBPs). (See also [22, 23] for similar ideas in the context of other clustering models, and more recent works [24, 25].) The significant information gain can be achieved if the SBPs are calibrated at the field level [26–34], which allows one to break the degeneracies present in the correlation functions [19]. In addition, the EFT-based full-shape analysis with SBPs allows one to efficiently incorporate small scale information beyond the commonly used two-point clustering observables.

Until now, SBPs were calibrated using a combination of N-body simulations and the Halo Occupation Distribution (HOD) framework [35, 36] to map galaxies onto the N-body simulation output (see [37] for a review). Ref. [38] extended this to hydrodynamical simulations.

¹ Note that effect is different from the so-called prior projection effects, originally studied in [4, 7, 16], see also [17, 18] for recent discussions. The simulation-based priors eliminate these projection effects [19].

* ivanov99@mit.edu

Given a dependence of SBPs on computationally expensive simulations, it is desirable to develop an analytic approach to SBPs, which could reduce their computational cost. In addition, such an approach should provide insights into the physics behind the EFT parameters, increasing the interpretability of the EFT-SBP results. This is especially relevant in light of the nominal power of this approach in constraining cosmological parameters [19, 21]. We address these questions in our note.

Our main aim is to use the halo model formalism [39–41] to predict the relations between the EFT parameters of dark matter halos and galaxies. These relations are well known for the galaxy bias parameters [42]. In this work we critically revisit the derivation of these expressions, and generalize these calculations to the case of redshift-space and stochasticity EFT parameters. Let us briefly introduce the key ingredients of our analytic approach using the known example of the galaxy bias parameters.

Galaxy and halo bias are functions encapsulating the dependence of the galaxy and halo overdensity $\delta_{h/g}$ on the underlying dark matter field δ_m (see [43] for a review). The bias expansion is formulated in terms of operators $\mathcal{O}_a(\mathbf{x})$ built out of the dark matter observables such as the tidal field. Schematically, the galaxy and halo bias expressions can be written as

$$\delta_h(\mathbf{x}) = \sum_{a=1} b_{\mathcal{O}_a}^h \mathcal{O}_a(\mathbf{x}), \quad \delta_g(\mathbf{x}) = \sum_{a=1} b_{\mathcal{O}_a}^g \mathcal{O}_a(\mathbf{x}), \quad (1)$$

where we have omitted the explicit time-dependence for brevity. The halo model predicts that the bias parameters of galaxies $b_{\mathcal{O}_a}^g$ are given by the bias parameters of halos weighted with the halo mass function $\bar{n}(M)$, and the mean halo occupation distribution $\langle N_g \rangle(M)$,

$$b_{\mathcal{O}_a}^g = \underbrace{\int d \ln M \bar{n}(M)}_{\text{halo mass function}} \underbrace{\langle N_g \rangle(M)}_{\text{galaxy-DM connection}} \underbrace{b_{\mathcal{O}_a}^h(M)}_{\text{Halo bias}}, \quad (2)$$

where the integral above is over the halo mass M . If we were to compute the bias parameters analytically, we would need three key ingredients.

The first ingredient is the halo mass function. Thanks to decades of intense theoretical efforts, many analytic results are readily available in the literature [44–46]. The second ingredient is the halo occupation distribution $\langle N_g \rangle(M)$ which captures the galaxy-dark matter connection. The basic theoretical HOD models such as [36] provide analytic formulas for $\langle N_g \rangle(M)$, which can be used to

do the integral (2) numerically. Finally, the last ingredient in the above formula is the bias parameter of halos as a function of the halo mass, $b_{\mathcal{O}_a}^h(M)$, or a related quantity of the halo model known as the “peak height” [39]. Since there are no available analytic results for all of the relevant EFT parameters for dark matter halos, in practice one has to extract $b_{\mathcal{O}_a}^h(M)$ from N-body simulations. However, these dependencies have to be calibrated from the simulations only once.

All in all, with the three ingredients described above, the halo mass function model, the analytic expression for the HOD function, and the halo bias as a function of the halo mass, one can compute the HOD-based galaxy bias parameters analytically. Our goal here is to carry out this computation explicitly, and extend this argument to other EFT parameters. Finally, we will compare the results against numerical simulations.

The analytic approach described above introduces some uncertainties. First, it relies on an analytic halo mass function model, which is always an approximation [46, 47]. Second, it uses the analytic form of the HOD that ignores important physical effects such as assembly bias [48]. Third, it assumes that the bias parameters of halo depends only on the mass, which is known to be violated in N-body simulations [49, 50]. Nevertheless, despite these drawbacks, our approach provides an economic way to generate the EFT priors analytically, and explore the dependence of the EFT parameters on the galaxy-halo connection parameters and the cosmological parameters. Note that priors do not need to be very accurate, i.e. the $\sim 10\%$ uncertainties are acceptable. Given that the currently used conservative priors allow for $\sim 100\%$ uncertainties on the EFT parameters and their correlations [6, 51, 52], reducing them to $\sim 10\%$ is already a dramatic improvement.

The rest of our note is structured as follows. Section 2 introduces the theoretical background on the galaxy parameters in the halo model and presents new expressions for the redshift-space and stochastic EFT parameters. We compare our analytic results against simulations in Section 3. The dependence of HOD-based priors on cosmological and HOD parameters is studied in Section 4. Section 5 draws conclusions.

2. THEORY

Let us describe now three key ingredients of our analytic approach. We start with the halo mass function.

2.1. Halo mass function

The halo mass function (HMF) computes the number density of halos of a given mass. Historically, it was first analytically derived by Press and Schechter [44]. Within the Press-Schechter (PS) approach, a halo is formed at a given point in space if the variance of the Lagrangian matter density fluctuation in a spherical cell around this point at the initial time slice was above a spherical collapse threshold. Using the Lagrangian density formally evolved to redshift zero, its variance inside a spherical cell around the point of interest is given by²

$$\sigma^2(R, z=0) = \int_{\mathbf{k}} P_{11}(k) W_{\text{th}}^2(kR), \quad (3)$$

where R is comoving, i.e. redshift-independent Lagrangian scale, W_{th}^2 is the Fourier image of the position space top-hat window of radius R , and $P_{11}(k)$ is the linear matter power spectrum at redshift zero. The mass variance at a finite redshift z is obtained by multiplying the above expression by the square of the linear growth factor $D_+(z)$:

$$\sigma^2(R, z) = D_+^2(z) \sigma^2(R, z=0). \quad (4)$$

The PS formalism assumes that the spherically averaged density field in a matter-dominated universe follows a non-linear spherical collapse evolution.³ In the spherical collapse model it is customary to use the linear theory density field as a proxy for time. The collapse of spherical shells (shell crossing) happens when the linear theory prediction formally reaches the threshold value $\delta_c = 1.686$, known as “critical density.” Given that the time-evolution is self-similar, shell crossing at redshift z happens in regions whose linear mass r.m.s. $\sigma(R, z)$

crosses the same threshold value δ_c . The PS model assumes that shell-crossing is followed by the creation of a halo. In this case, the HMF is given by

$$\bar{n}(M) \equiv \frac{d\bar{n}(M, z)}{d \ln M} = \frac{\bar{\rho}_m(t_0)}{M} \left| \frac{d \ln \sigma(M, z)}{d \ln M} \right| \nu f(\nu), \quad (5)$$

$$f(\nu) = \sqrt{\frac{2}{\pi}} \exp\{-\nu^2/2\},$$

where the key parameter that controls the HMF is

$$\nu = \frac{\delta_c}{\sigma(M[R], z)}, \quad (6)$$

which we call the “peak height.” (Note that [54] uses the same term for ν^2 .) The principal dependence of the HMF only on the combination ν implies *universality*: a rescaling of the HMF by redshift can be fully compensated by a shift of its mass. Consequently, this implies a self-similar shape of the HMF.

Going beyond the matter dominated universe within the PS framework, the cosmology dependence is controlled by the same combination ν . Just as before, σ^2 captures the initial conditions and the evolution prior to the onset of structure formation, while δ_c is promoted to depend on the time-dependent matter abundance

$$\Omega_m(z) = \frac{\Omega_{m,0}(1+z)^3}{\Omega_{m,0}(1+z)^3 + 1 - \Omega_{m,0}}, \quad (7)$$

where $\Omega_{m,0}$ is the matter abundance at $z=0$, as [55]

$$\delta_c = \frac{3}{20} (12\pi)^{2/3} (1 + 0.0123 \log \Omega_m(z)). \quad (8)$$

The PS HMF has been generalized in multiple ways. The first popular extension is the Sheth-Torman mass function (ST HMF) [45], which accounts for the ellipsoidal collapse,

$$f_{\text{ST}}(\nu) = A \left[1 + \frac{1}{(a\nu)^p} \right] \sqrt{\frac{a}{2\pi}} \exp\{-\nu^2/2\}, \quad (9)$$

with $p=0.3$ and $a=0.707$. A is determined through the normalization condition that all matter in the Universe is contained in halos,

$$\int d\nu f_{\text{ST}}(\nu) = 1. \quad (10)$$

Another popular generalization is the Tinker mass function (THMF) [46], which is a fit to simulations,

$$f_{\text{T}}(\nu) = \alpha [1 + (\beta\nu)^{-2\phi}] \nu^{2\eta} e^{-\gamma\nu^2/2}, \quad (11)$$

² We use the notation $\int_{\mathbf{k}} \equiv \int d^3k$.

³ This is true for the spherically averaged overdensity in the statistical sense since the path integral of the spherically averaged matter density probability distribution function is dominated by a spherical collapse saddle point [53].

with

$$\begin{aligned}\beta &= 0.589(1+z)^{0.20} \\ \phi &= -0.729(1+z)^{-0.08} \\ \eta &= -0.243(1+z)^{0.27} \\ \gamma &= 0.864(1+z)^{-0.01},\end{aligned}\tag{12}$$

and α is again determined from eq. (10). In all these cases the universal shape of the mass function is preserved.

The universality has been extensively tested with N-body simulations. While the corrections have been detected, in general they are very small, especially for cosmology variations allowed by current experiment [47]. In what follows we will assume the universality of the HMF and use the THMF in all practical calculations.

2.2. EFT parameters of halos

The second ingredient of our approach is the set of EFT parameters of dark matter halos. Let us discuss the various kinds of EFT parameters one-by-one.

1. Bias parameters

The EFT Eulerian bias model relevant for the description of the halo power spectrum at the one-loop order reads [43, 56],

$$\delta_g^{\text{EFT}}(\mathbf{k}) = b_1^h \delta + \frac{b_2^h}{2} \delta^2 + b_{\mathcal{G}_2}^h \mathcal{G}_2 + b_{\Gamma_3}^h \Gamma_3 - b_{\nabla^2 \delta}^h \nabla^2 \delta + \epsilon, \tag{13}$$

where δ is the non-linear matter density field, \mathcal{G}_2 is the tidal operator,

$$\begin{aligned}\mathcal{G}_2(\mathbf{k}) &= \int_{\mathbf{p}} F_{\mathcal{G}_2}(\mathbf{p}, \mathbf{k} - \mathbf{p}) \delta(\mathbf{p}) \delta(\mathbf{k} - \mathbf{p}), \\ F_{\mathcal{G}_2}(\mathbf{k}_1, \mathbf{k}_2) &= \frac{(\mathbf{k}_1 \cdot \mathbf{k}_2)^2}{k_1^2 k_2^2} - 1,\end{aligned}\tag{14}$$

$\int_{\mathbf{k}} \equiv \int \frac{d^3 \mathbf{k}}{(2\pi)^3}$ and Γ_3 is the Galileon cubic tidal operator,

$$\begin{aligned}\Gamma_3 &= \int_{\mathbf{k}_1} \int_{\mathbf{k}_2} \int_{\mathbf{k}_3} \left(\prod_{i=1}^3 \delta(\mathbf{k}_i) \right) (2\pi)^3 \delta_D^{(3)}(\mathbf{k} - \mathbf{k}_{123}) F_{\Gamma_3}, \\ F_{\Gamma_3} &= \frac{4}{7} \left(1 - \frac{(\mathbf{k}_1 \cdot \mathbf{k}_2)^2}{k_1^2 k_2^2} \right) \left(\frac{((\mathbf{k}_1 + \mathbf{k}_2) \cdot \mathbf{k}_3)^2}{(\mathbf{k}_1 + \mathbf{k}_2)^2 k_3^2} - 1 \right).\end{aligned}\tag{15}$$

The field ϵ in eq. (13) is a stochastic density component.

In perturbation theory [57] one expands the non-linear matter field δ in expressions above through the linear density field, schematically

$$\delta = \delta_1 + \int F_2 \delta_1^2 + \delta_{\text{ctr.}} + \dots \tag{16}$$

$\delta_{\text{ctr.}} = -c_s^2 k^2 \delta_1$ above is the counterterm contribution needed to account for the backreaction from small scales. At leading order it produces a contribution indistinguishable from the higher-derivative bias, so in what follows it will be convenient to re-define

$$b_{\nabla^2 \delta}^h = b_{\nabla^2 \delta}^h - b_1 c_s, \tag{17}$$

as this is the combination that appears in all the calculations at the one-loop power spectrum order that we use here.

The bias expression (13) describes the correlation of the halo overdensity with the underlying matter field. Let us discuss briefly now how this expression appears in the halo model [43]. The formation of halos is modulated by long-wavelength modes, which act as a background on the proto-halos. This leads to correlations of the positions of halos and the cosmological fluctuations on large scales, captured by the local in the density field bias relation

$$\delta_h^L(\mathbf{x}_L) = \frac{n(\mathbf{x}_L)}{\bar{n}} - 1 = b_1^L \delta_m(\mathbf{x}_L) + \frac{b_2^L(\mathbf{x}_L)}{2} \delta_m^2 + \dots, \tag{18}$$

where \mathbf{x}_L is the Lagrangian coordinate of the initial time slice. At the linear level this leads to the Eulerian bias relation

$$\delta_h(\mathbf{x}, z) = b_1^h \delta_m(\mathbf{x}, z) \tag{19}$$

where $b_1^h = b_1^L + 1$ is the linear bias parameter. In the simplest models of the halo formation, such as the peak-background split, b_1 depends only ν by virtue of the HMF universality. Analytic results have been derived for the linear bias in the context of the PS and ST HMFs [58]:

$$\begin{aligned}b_1^{\text{PS}}(\nu) &= 1 + \frac{\nu^2 - 1}{\delta_c}, \\ b_1^{\text{ST}}(\nu) &= 1 + \frac{1}{\delta_c} \left(a\nu^2 - 1 + \frac{2p}{1 + (a\nu^2)^p} \right).\end{aligned}\tag{20}$$

Note that we have added the unity to the above expressions to convert the Lagrangian bias predicted by the peak background split model into the observationally relevant Eulerian bias. For the THMF, the fit to simulation data reads [59]:

$$b_1(\nu) = 1 - A \frac{\nu^a}{\nu^a + \delta_c^a} + B \nu^b + C \nu^c, \tag{21}$$

where $y = \log(200)$ and

$$\begin{aligned} A &= 1 + 0.24y \exp(-(4/y)^2), \\ a &= 0.44y - 0.88, \\ B &= 0.183, \\ b &= 1.5, \\ C &= 0.019 + 0.107y + 0.19 \exp(-(4/y)^2), \\ c &= 2.4. \end{aligned} \quad (22)$$

We note that this fit was calibrated to reproduce the linear bias in the range $\ln \nu \in [-0.3, 0.5]$ within $\lesssim 20\%$. Analogous expressions have been obtained for higher order local in density field bias parameters, e.g.

$$\begin{aligned} b_2^{\text{ST}}(\nu)|_L &= \frac{1}{\delta_c^2} \left(a^2 \nu^4 - 3a\nu^2 + \frac{2p(2a\nu^2 + 2p - 1)}{1 + (a\nu^2)^p} \right) \\ b_2 &= b_2|_L + \frac{8}{21}(b_1 - 1) + \frac{4}{3}b_{\mathcal{G}_2} = b_2|_L + \frac{4}{3}b_{\mathcal{G}_2}|_L, \end{aligned} \quad (23)$$

where $b_{\mathcal{G}_2}|_L$ is the Lagrangian tidal bias. The PS prediction can be recovered by setting $a = 1, p = 0$.

Within the local-in-the-density-field Lagrangian bias model the Lagrangian bias is assumed to be local cf. (18), as follows from the PBS arguments. All other terms in the EFT expression (13) are generated by the mapping from Lagrangian to Eulerian spaces. In particular, the tidal bias satisfies

$$b_{\mathcal{G}_2} = -\frac{2}{7}(b_1 - 1). \quad (24)$$

This picture is known to be oversimplified, as the Lagrangian halo bias in simulations also depends on the tidal fields, as well as the higher derivative terms [32, 60].

In the basic formulation of the halo model the bias parameters of halos depend only on the halo mass through the parameter ν . This parameter also captures the cosmology dependence. Within this framework, it is natural to expect then that other bias parameters, such as $b_{\mathcal{G}_2}$, b_{Γ_3} , $b_{\nabla^2\delta}$ etc. primarily depend on the masses and cosmology through peak height ν as well. Since the analytic results for these bias parameters as functions of ν are not available, we will use the dependencies extracted from simulations. This applies to $b_1(\nu)$ and $b_2(\nu)$ as well, as in the analytic formulas presented above work only within $\sim 10\%$ precision [61].

In fig. 1 we show the bias parameters of dark matter halos as a function of ν extracted from 10 *Quijote* fiducial simulations in ref. [19] at $z = 0.5$. We use the friends-of-friends halo catalogs. Since the cosmological parameters

are fixed in this case, the variation of ν corresponds to the variation of the halo mass. As anticipated, all bias parameters exhibit clear correlations with ν . We use cubic splines to interpolate these dependencies. The interpolated functions $b_{\mathcal{O}_a}(\nu)$ ($\mathcal{O}_a = \{\delta, \frac{1}{2}\delta^2, \mathcal{G}_2, \Gamma_3, b_{\nabla^2\delta}\}$) will be then used to express the bias parameters as functions of mass.

For b_1 we also show the predictions of the STHMF and THMF, while for b_2 we show the STHMF result (23) where $b_{\mathcal{G}_2}$ is determined by the local Lagrangian prediction. We can see that for b_1 the agreement between the analytic formulas and measurements are quite decent, but as expected, it quickly deteriorates for $\nu > 2$. As for b_2 , the performance of the analytic prediction based on the Sheth-Tormen HMF is quite poor for the entire range of masses.

As far as the higher derivative counterterm $b_{\nabla^2\delta}$ is concerned, we have previously found that its dependence on ν is halo-finder specific [19].⁴ In order to match our previous HOD-based results from the *AbacusSummit* simulation more directly, we use the $b_{\nabla^2\delta}(\nu)$ measurements based on the same halo definition. Specifically, we measure $b_{\nabla^2\delta}(\nu)$ from a single box of *Abacus small* suite (site length of $500 h^{-1}\text{Mpc}$) for halo catalogs created with the CompaSO halo finding algorithm [62]. While the use of the small *Abacus* box leads to a somewhat large statistical scatter for large values of ν , this affects our EFT parameter predictions only at a $\sim 10\%$ level, which is within the target error budget.⁵ Note that one important feature of $b_{\nabla^2\delta}$ which we recover both in *AbacusSummit* and *Quijote* is its turnover at $\nu \approx 2$, see the bottom right panel of fig. 1. This turnover is consistent with the previous measurements by [32].

2. Stochasticity parameters

In the halo model, the stochastic contributions are captured by the one-halo term. In the first approximation,

⁴ Note that we have also found some halo-finder dependence for the usual bias parameters of halos as well [19]. However, this dependence is much weaker than that of the counterterms, and we stick to the *Quijote* measurements for the bias parameters in order to reduce the statistical noise in the $b_{\mathcal{O}_a}(\nu)$ relations.

⁵ In principle, this can be improved by combining more boxes or using the baseline *AbacusSummit* simulations. This is, however, not required for our current precision goal.

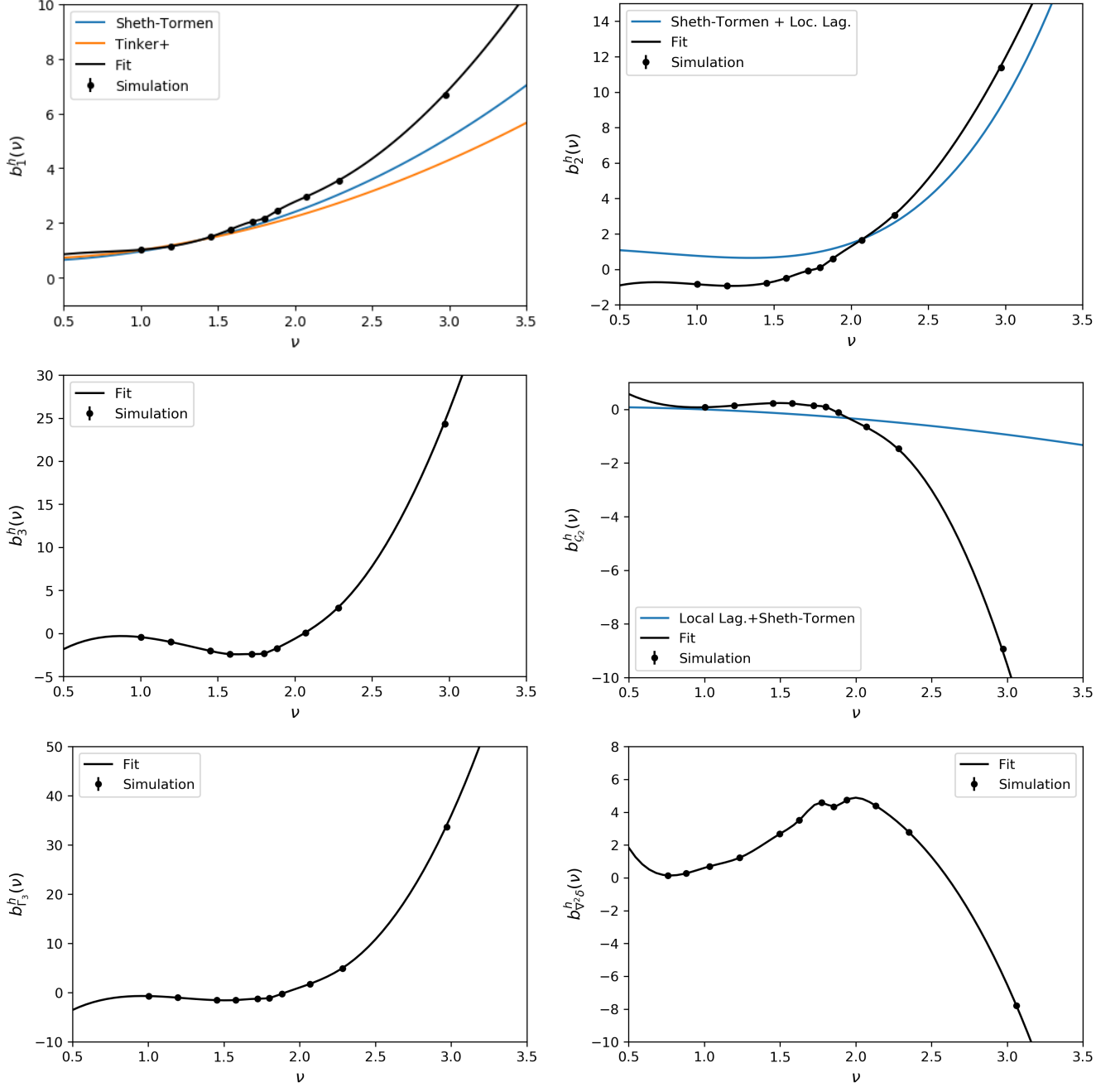


FIG. 1. EFT parameters of halos as a function of the peak height ν . Some analytic models for $b_1(\nu)$ and $b_2(\nu)$ are shown for comparison. Dots represent measurements from N-body simulations, while the solid lines are cubic spline fits.

the stochastic power spectrum of halos can be approximated as Poissonian. In general, halos exhibit departures from the Poissonian stochasticity due to exclusion effects [63]. These departures manifest themselves in the change of the overall amplitude of the constant contribution, and the appearance of the scale-dependence. These are captured within EFT by the following stochas-

tic counterterms

$$\begin{aligned} \langle \varepsilon(\mathbf{k}) \varepsilon(\mathbf{k}') \rangle &= (2\pi)^3 \delta_D^{(3)}(\mathbf{k} + \mathbf{k}') P_{\text{stoch}} \\ P_{\text{stoch}} &= \frac{1}{\bar{n}} \left(1 + \alpha_0 + \alpha_1 \left(\frac{k}{k'_{\text{NL}}} \right)^2 \right), \end{aligned} \quad (25)$$

where $k'_{\text{NL}} = 0.45 \, h\text{Mpc}^{-1}$ following [51, 64]. Under our baseline assumption that the peak height is the only parameter that controls the stochasticity of halos, we

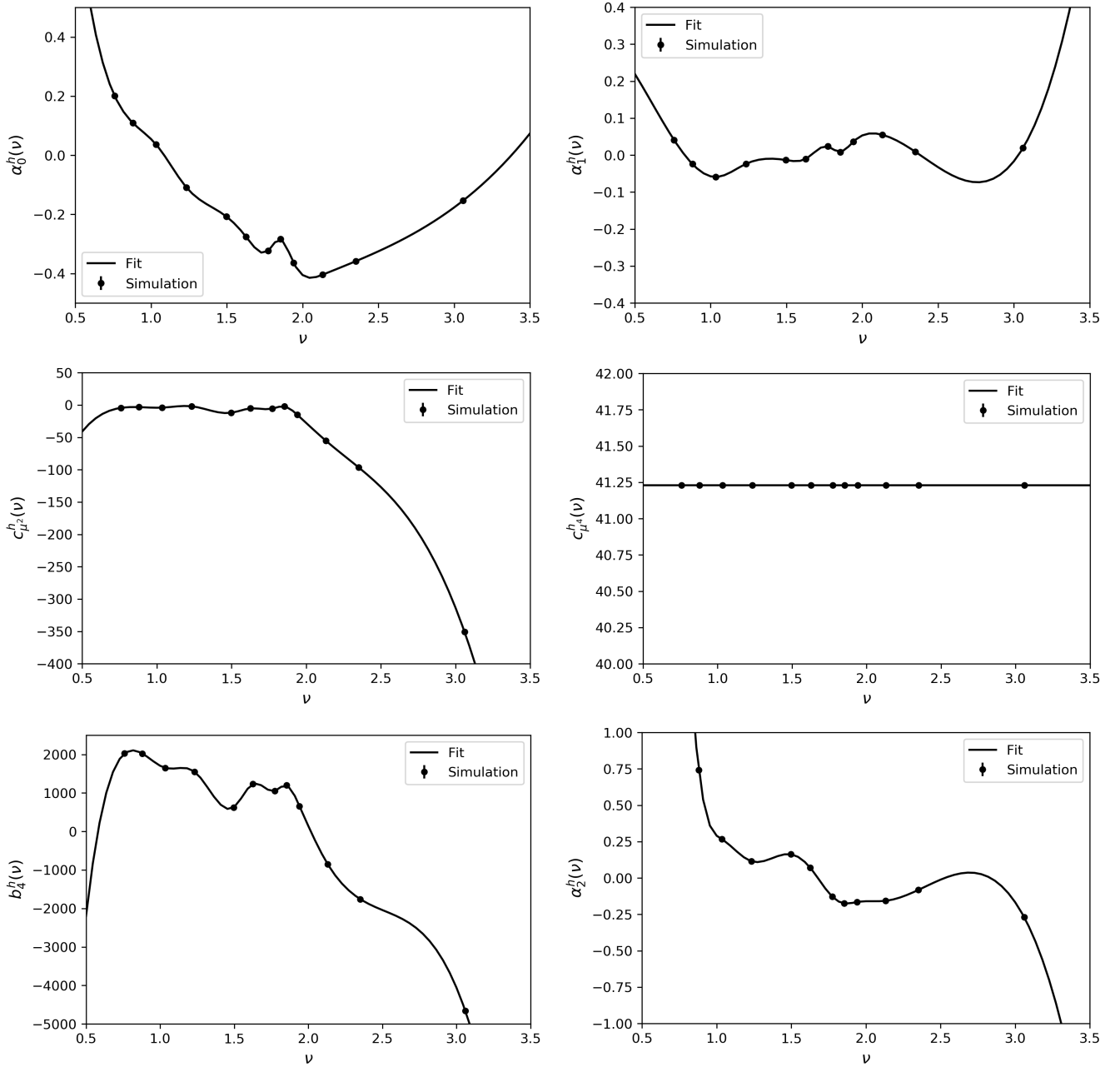


FIG. 2. EFT stochastic parameters and redshift-space counterterms of halos as a function of the peak height ν .

can extract the functions $\alpha_{0,1}(\nu)$ from the **Abacus small** CompaSO halo catalog, see the bottom panel of fig. 2. In agreement with the expected exclusion effects, we see that the low mass halos exhibit super-Poissonian stochasticity, while the large mass halos' stochasticity is sub-Poissonian [33, 63]. We also find that the scale-dependent stochasticity is negative for low mass halos, but it changes the sign and grows quickly for large halo masses.

3. RSD counterterms

In EFT, the RSD counterterms appear as a result of the renormalization of local products of the density and velocity fields that stem from the redshift-space mapping. Expanding this mapping perturbatively we obtain the following expression for the halo density field in redshift

space [65, 66]:

$$\begin{aligned} \delta_h^{(s)}(\mathbf{k}) = & \delta(\mathbf{k}) - \frac{ik_z}{\mathcal{H}} v_{h,z}(\mathbf{k}) - \frac{(ik_z)^2}{2\mathcal{H}^2} [v_{h,z}^2]_{\mathbf{k}} \\ & - \frac{i^3}{3!} \left(\frac{k_z}{\mathcal{H}} \right)^3 [v_{h,z}^3]_{\mathbf{k}} - \frac{ik_z}{\mathcal{H}} [v_{h,z} \delta_h]_{\mathbf{k}} + \frac{(ik_z)^2}{2\mathcal{H}^2} [\delta_h v_{h,z}]_{\mathbf{k}} , \end{aligned} \quad (26)$$

where $\mathcal{H} = aH$ and v_h is the halo velocity field. Subscripts z denote projections onto the line-of-sight z . This renormalization can be thought of as a result of coarse-graining of the local products of the fields, and practically it amounts to replacing the relevant products above as follows [65]

$$\begin{aligned} \mathcal{H}^{-1}[v_{h,z} \delta_h]_{\mathbf{k}} & \rightarrow \mathcal{H}^{-1}[v_{h,z} \delta_h]_{\mathbf{k}} + ic_4 k_z \delta_h \\ \mathcal{H}^{-2}[v_{h,z}^2]_{\mathbf{k}} & \rightarrow \mathcal{H}^{-2}[v_{h,z}^2]_{\mathbf{k}} + c_2 \delta + c_3 \frac{k_z^2}{k^2} \delta_m, \\ \mathcal{H}^{-3}[v_{h,z}^3]_{\mathbf{k}} & \rightarrow \mathcal{H}^{-3}[v_{h,z}^3]_{\mathbf{k}} + 3c_1 v_z, \\ \mathcal{H}^{-2}[v_z^2 \delta_h] & \rightarrow \mathcal{H}^{-2}[v_z^2 \delta_h] + c_5 \delta_h. \end{aligned} \quad (27)$$

Note that at leading order $v_h = v_m$, so that the counterterms $c_{1,2,3}$ are the same for halos and dark matter thanks to the equivalence principle. For the linear velocity term in eq. (27) we should also take into account its renormalization due to the dark matter velocity counterterm

$$\theta = \theta^{(1)} + k^2 c_\theta \delta^{(1)}. \quad (28)$$

In addition, there is a halo-specific velocity bias [43]

$$\theta = \theta^{(1)} + k^2 b_{\nabla^2 \mathbf{v}} \delta^{(1)}, \quad (29)$$

where the upper script (1) means that the corresponding fields should be evaluated in linear theory. Combining all contributions together, one obtains the following expression for the halo redshift space counterterm

$$\delta_{\text{ctr}}^{(s)} = (c_{\mu^2} f \mu^2 + c_{\mu^4} f^2 \mu^4) k^2 \delta^{(1)}, \quad (30)$$

where

$$\begin{aligned} f c_{\mu^2} & \equiv (c_4 - \frac{1}{2} c_5) b_1 - \frac{c_2}{2} + f c_\theta + f b_{\nabla^2 \mathbf{v}}, \\ f^2 c_{\mu^4} & \equiv \frac{1}{2} (f c_1 - c_3). \end{aligned} \quad (31)$$

The c_{μ^4} counterterm is the same for halos and dark matter. In contrast, the c_{μ^2} counterterm depends both on cosmology and halo properties.

Redshift-space clustering of matter and halos is subject to the non-linear smearing of power due to virial motions known as the finger-of-God effect [67]. In the

EFT this leads to an enhancement of the EFT cutoff in redshift space and an early breakdown of the one-loop EFT model [4, 64, 68]. One can improve the agreement between the one-loop EFT calculation and data by including the higher order counterterms in the calculation, which capture the enhanced fingers-of-God. Following refs. [4], we parameterize them as

$$\delta_{\delta_z^4 \delta}^{(s)} = -\frac{b_4^h}{2} f^4 \mu^4 k^4 (b_1 + f \mu^2) \delta^{(1)}, \quad (32)$$

Finally, there is a stochastic RSD counterterm parameterized by α_2 :

$$P_{\text{stoch}} = \frac{1}{\bar{n}} \left(1 + \alpha_0 + \alpha_1 \left(\frac{k}{k'_{\text{NL}}} \right)^2 + \alpha_2 \mu^2 \left(\frac{k}{k'_{\text{NL}}} \right)^2 \right), \quad (33)$$

where $k'_{\text{NL}} = 0.45 \text{ hMpc}^{-1}$ as before.

In fig. 2 we show the RSD counterterms c_{μ^2} , c_{μ^4} , α_2 and b_4 as functions of ν extracted from the halo data. These counterterms appear to be rather complicated, non-monotonic functions of ν . Note that for the c_{μ^4} fit we have included the dark matter field-level results as well in order to reduce the scatter of measurements from large mass bins.

2.3. HOD galaxies

Within the HOD model, each halo can host galaxies that follow specific probability distributions. In the simplest realization of these ideas, the halo mass is the only parameter that determines the number of galaxies. The host galaxies are split into centrals and satellites. Each halo hosting a galaxy has exactly one central galaxy which is located in the vicinity of the center of mass of the halo. All other galaxies within the same halo are called satellites. Each halo then is assigned a random variable of galaxies N_g , which is given by the sum of the central galaxy N_c (taking the values 0 or 1) and the satellite N_s , which is expressed as $N_s = N_c \mathcal{N}_s$ since the probability to have a satellite galaxy is conditioned on having a central. The mean number density of galaxies is given by

$$\bar{n}_g = \int d \ln M \bar{n} \langle N_g \rangle_M \quad (34)$$

where $\langle N_g \rangle_M$ is the average halo occupation distribution,

$$\langle N_g \rangle_M = \langle N_c \rangle_M + \langle N_c \rangle_M \langle \mathcal{N}_s \rangle_M. \quad (35)$$

Note that we made an assumption that the HOD depends only on the halo mass. In particular, it is independent of the background cosmology. In addition, we will assume that \mathcal{N}_s follows a Poisson distribution.

1. Galaxy bias

Perturbations in the halo number density

$$n(M, \mathbf{x}) = \bar{n}(M)(1 + \delta_h(\mathbf{x})). \quad (36)$$

lead to perturbations in the galaxy density,

$$\begin{aligned} n_g(\mathbf{x}) &= \bar{n}_g(1 + \delta_g(\mathbf{x})) \\ &= \int d \ln M \bar{n}(M) \langle N_g \rangle_M (1 + \delta_h(\mathbf{x})). \end{aligned} \quad (37)$$

Removing the background quantities we find

$$\delta_g(\mathbf{x}) = \frac{1}{\bar{n}_g} \int d \ln M \bar{n}(M) \langle N_g \rangle_M \delta_h(\mathbf{x}), \quad (38)$$

which implies the known relation between the bias parameters of halos and galaxies [25, 42],

$$b_{\mathcal{O}_a}^g = \frac{1}{\bar{n}_g} \int d \ln M \bar{n}(M) \langle N_g \rangle_M b_{\mathcal{O}_a}^h(M). \quad (39)$$

Note that within the HOD model the above expression is often modified by the galaxy or halo profile function $u(k)$. But the perturbative bias expansion that we use is applicable only on large scales, i.e. the limit $k \rightarrow 0$ where $u(k) \rightarrow 1$, which recovers eq. (39).⁶

The shape of $\langle N_g \rangle_M$ is modeled phenomenologically. In the simplest case, one assumes the following parameterization for the luminosity-limited galaxy samples, such as Luminous Red Galaxies [36],

$$\begin{aligned} \langle N_c \rangle &= \frac{1}{2} \left[1 + \text{Erf} \left(\frac{\log M - \log M_{\text{cut}}}{\sqrt{2}\sigma} \right) \right], \\ \langle \mathcal{N}_s \rangle &= \Theta_H(M - \kappa M_{\text{cut}}) \left(\frac{M - \kappa M_{\text{cut}}}{M_1} \right)^\alpha. \end{aligned} \quad (40)$$

This basic HOD model is parameterized by five free parameters M_{cut} , σ , M_1 , κ and α plus two velocity bias parameters that we will discuss shortly.

Note that there is an evidence that the basic HOD model fails to correctly capture the clustering even for the luminosity-limited galaxy samples, see e.g. [48, 69–72]. HOD extensions with concentration and density-dependent assembly bias provide a better description of the hydrodynamical simulations and the data. Such extensions are referred to as “decorated” HOD models [48]. The failure of the minimal HOD is the main reason why realistic HOD-based EFT parameter samples applied to data have been produced using the decorated HODs [19, 21]. In what follows, however, we will use only this basic HOD parameterization that allows for a simple analytic treatment.

2. Redshift space counterterms and velocity bias

Note that in redshift space, the density field in eq. (38) is subjected to redshift-space mapping. Then one Taylor expands the mapping in the EFT to arrive at the expressions of the type (see eq. (27)):

$$v_g^z(\mathbf{x}) \delta_g(\mathbf{x})|_{\text{ren.}} = v^z(\mathbf{x}) \delta_g(\mathbf{x}) - c_4^g \mathcal{H} \nabla_z \delta_m^{(1)}(\mathbf{x}), \quad (41)$$

where for convenience we switched to position space. Let us first assume that there is no velocity bias, i.e. $\mathbf{v}_g = \mathbf{v}$, so that all galaxies are simply co-moving with the halos. This should be satisfied on large scales thanks to the equivalence principle. Then, in the HOD model

$$v_z \delta_g|_{\text{ren.}} = \int dM \frac{d\bar{n}}{dM} v_z \delta_h|_{\text{ren.}}, \quad (42)$$

which implies

$$c_4^g = \frac{1}{\bar{n}_g} \int dM \frac{d\bar{n}}{dM} \langle N_g \rangle c_4^h(M), \quad (43)$$

i.e., all halo-dependent counterterms get weighted by the HOD. We stress that so far we have ignored the velocity bias. We conclude that the HOD framework predicts that the redshift-space counterterms of galaxies is inherited from halos. Since the dark matter counterterms do not depend on the halo mass, we find

$$c_{1,2,3} = \frac{1}{\bar{n}_g} \int dM \frac{d\bar{n}}{dM} \langle N_g \rangle c_{1,2,3}. \quad (44)$$

Hence, they can be added to eq. (43) so that we get the following expression for the total redshift space counterterm

$$c_{\mu^2}^g|_{\text{halo}} = \frac{1}{\bar{n}_g} \int dM \frac{d\bar{n}}{dM} \langle N_g \rangle c_{\mu^2}^h(M). \quad (45)$$

⁶ In principle, the Taylor expansion of $u(k)$ produces k^2 corrections on large scales that modifies the higher derivative bias $b_{\nabla^2 \delta}$. In practice, however, we find that these corrections are negligibly small so we ignore them in what follows.

The above equation describes the contribution to the RSD counterterm that galaxies “inherit” from the halos.

In addition to eq. (45), there is a contribution due to velocity bias w.r.t. dark matter particles within the halo, which we denote as $c_{\mu^2}^g|_{\text{vel}}$. Physically, they arise because galaxies are moving w.r.t. the halo center of mass due to the virial potential within the halo. The basic halo models describe such motions by means of the Gaussian convolution of the density field in redshift space [41],

$$\begin{aligned}\delta_g^{(s)} &= (b_1 + f\mu^2)\delta_m e^{-\frac{\Sigma_M^2 \mu^2 k^2}{2}} \\ &= (b_1 + f\mu^2)\delta_m - \frac{k^2}{2}(b_1 \Sigma_M^2 \mu^2 + f \Sigma_M^2 \mu^4)\delta_m \\ &\quad + \frac{(k\mu \Sigma_M)^4}{8}(b_1 + f\mu^2)\delta_m + \dots\end{aligned}\quad (46)$$

The above Gaussian filter is determined by the mass-dependent 1-dimensional velocity dispersion [73],

$$\Sigma_M = \left(\frac{GM}{2r_{\text{vir}}}\right)^{1/2}. \quad (47)$$

Eq. (46) describes the smearing of the density inside the halo. Without velocity bias, the centrals are co-moving with the halo centers of mass, so the smearing is produced only by the satellites. The $k^2 \mu^2$ counterterm of galaxies then follows from the HOD weighting of the above velocity dispersion [40, 73, 74],

$$\begin{aligned}\delta_g^{(s)} &= \int dM \frac{d\bar{n}}{dM} \langle N_s \rangle \delta^{(s)} \\ &\supset -\frac{k^2 \mu^2}{2} \int dM \frac{d\bar{n}}{dM} \langle N_s \rangle b_1^h(M) \Sigma_M^2.\end{aligned}\quad (48)$$

In the HOD framework the velocity of galaxies is shifted from the velocity dark matter particles by the velocity bias α_c , and α_s parameters, respectively [35, 75],

$$\begin{aligned}\mathbf{v}_c &= \mathbf{v}_h + \alpha_c(\mathbf{v}_m - \mathbf{v}_h), \\ \mathbf{v}_s &= \mathbf{v}_h + \alpha_s(\mathbf{v}_m - \mathbf{v}_h),\end{aligned}\quad (49)$$

where \mathbf{v}_h is the halo center-of-mass velocity, and \mathbf{v}_m is the velocity of dark matter particle inside the halo. The case $\alpha_c = 0$, $\alpha_c = 1$ reproduces the common assumption of the basic halo model that the centrals are co-moving with the halo centers of mass, while the satellites are moving with the typical velocities of the host dark matter particles. Due to the velocity bias, the velocity dispersion of galaxies is different from the matter velocity dispersion,

$$\Sigma_{c/s}^2 = \alpha_{c/s}^2 \Sigma_M^2. \quad (50)$$

Note that due to the velocity bias the density component produced by the centrals gets smeared as well. Including the velocity bias and extending eq. (48) to the centrals we arrive at the final expression

$$\begin{aligned}c_{\mu^2}^g|_{\text{vel.}} &= -\frac{1}{2f\bar{n}_g} \int dM \frac{d\bar{n}}{dM} b_1^h(M) \\ &\quad \times [\langle N_c \rangle \alpha_c^2 + \langle N_s \rangle \alpha_s^2] \Sigma_M^2.\end{aligned}\quad (51)$$

The total $\mu^2 k^2 \delta_m$ counterterm coefficient is the sum of the halo one and the one produced by the virialized velocity dispersion,

$$c_{\mu^2} = c_{\mu^2}|_{\text{halo}} + c_{\mu^2}|_{\text{vel.}}. \quad (52)$$

In passing, we note that the halo model expression (46) predicts that the coefficient in front of $k^2 \mu^4$ term is mass dependent,

$$c_{\mu^4} = -\frac{1}{2f} \Sigma_M^2. \quad (53)$$

The non-universality of this term clashes with the EFT prediction dictated by the equivalence principle. This is another limitation of the halo model, which appears to violate the equivalence principle in addition to the mass and momentum conservation.

Let us discuss now the higher-order k^4 counterterm parameterized by the constant b_4 . Just like the $\mu^2 k^2$ counterterm, the $\mu^4 k^4$ counterterm also consists of two pieces,

$$b_4^g = b_4^g|_{\text{halo}} + b_4^g|_{\text{vel.}} \quad (54)$$

The first piece is inherited from the dark matter halos,

$$b_1^g b_4^g|_{\text{halo}} = \frac{1}{\bar{n}_g} \int dM \frac{d\bar{n}}{dM} \langle N_g \rangle b_1^h(M) b_4^h(M). \quad (55)$$

The second term $b_4^g|_{\text{vel.}}$ is generated by the velocity bias, and can be obtained by Taylor expanding the Gaussian smearing kernel in eq. (46) up to quadratic order. We note, however, that at this order the phenomenological models available in the literature start to give different predictions. The Gaussian model gives a coefficient 1/8 in front of the $(k\mu \Sigma_M)^4$ term, but the other popular Lorentzian model of the fingers-of-God damping [76] gives the coefficient 3/16. More generally, one expects a more complicated fingers-of-God damping function modified by the higher order moments of the virialized velocity field [77–79]. In this work we stick to the simplest model

where the only relevant parameter is the velocity dispersion, and use our flexibility in the choice of the coefficient in front of the $(k\mu\Sigma_M)^4$ to set it to 1/16, preferred by the field-level transfer function data from [19]. Taking this model and rescaling the velocity dispersion by the appropriate velocity bias coefficients, we obtain

$$b_4^g|_{\text{vel.}} = -\frac{1}{8f^4b_1^g\bar{n}_g} \int dM \frac{d\bar{n}}{dM} \Sigma_M^4 b_1^h(M) \times [\langle N_c \rangle \alpha_c^4 + \langle N_s \rangle \alpha_s^4]. \quad (56)$$

It is interesting to note that the net correction to b_4 from the virialized motion is negative, which can be contrasted with $b_4^g|_{\text{halo}}$, which is positive for relatively light halos and negative for very massive ones, see fig. 2. Thus, the total sign of the b_4^g term can be both positive and negative depending on the HOD model.

Our results clarify the role of the satellites in limiting the range of validity of EFT in redshift space. The latter is determined by the amplitude of the EFT redshift space parameters. In the case of the basic HOD model (i.e. if we ignore the counterterm contributions inherited from halo), $\alpha_c = 0$ and $\alpha_s = 1$, i.e. the velocity dispersion of the satellites is the only source of the fingers-of-God. However, analyses of the galaxy samples with reduced satellite fractions [80, 81] showed that their removal does not significantly improve the reach of the one-loop EFT power spectrum predictions in redshift space. Our analysis shows that one reason for that is the RSD counterterm contribution inherited from the halos, eq. (45). This contribution can be quite large even for the HODs with centrals only, especially if one is tracing massive halos.

3. Galaxy stochasticity

In the basic formulation of the halo model the stochasticity of halos and galaxies is captured by the correlations between galaxies within the same halo, encapsulated by one-halo term. Clearly, by construction this term can produce only the super-Poisson contribution [82],

$$\Delta P_{\text{stoch.}}^g = \frac{1}{\bar{n}_g^2} \int d\ln M \bar{n} \langle N_c \rangle (2\langle \mathcal{N}_s \rangle + \langle \mathcal{N}_s \rangle^2). \quad (57)$$

The stochasticity of the halos is assumed to be Poissonian and given by $1/\bar{n}$. Likewise, the stochasticity of the centrals is also given by the Poissonian prediction. In the halo model terminology this is a stochastic part of the two-halo term. Combined with the two-halo satellite

Poissonian prediction, this yields the standard answer \bar{n}_g^{-1} . Combining this with the one-halo satellite contribution (57), we get

$$P_{\text{stoch}}^g = \frac{1}{\bar{n}_g} + \frac{1}{\bar{n}_g^2} \int d\ln M \bar{n}_h \langle N_c \rangle (2\langle \mathcal{N}_s \rangle + \langle \mathcal{N}_s \rangle^2), \\ = \frac{1}{\bar{n}_g^2} \int d\ln M \bar{n}_h \langle N_c \rangle (1 + 3\langle \mathcal{N}_s \rangle + \langle \mathcal{N}_s \rangle^2). \quad (58)$$

While this equation does capture the basic fact that the galaxy stochasticity is different from the Poisson prediction, it misses the exclusion effects that produce the sub-Poissonian shot noise [63].

The proper inclusion of exclusion effects requires taking into account deterministic two-halo correlations. In ref. [63] this was done for the galaxy bias model including the Lagrangian quadratic bias. In principle, one could extend the approach of [63] to higher order biases [22, 76]. But even in this case the exclusion prediction depends on the galaxy correlation function on very small scales, which cannot be predicted analytically. Therefore, for the phenomenological reasons, we consider a simple modification of eq. (58) with the one-halo term replaced by its exclusion-corrected version from simulations,

$$P_{\text{stoch}}^g = \frac{1}{\bar{n}_g^2} \int d\ln M \bar{n} [\langle N_c \rangle \times (1 + 3\langle \mathcal{N}_s \rangle + \langle \mathcal{N}_s \rangle^2)(1 + \alpha_0(\nu[M]))], \quad (59)$$

implying

$$\tilde{\alpha}_0^g = \frac{1}{\bar{n}_g} \int d\ln M \bar{n} [\langle N_g \rangle \alpha_0(M) + (1 + \alpha_0(M))(2\langle N_c \rangle \langle \mathcal{N}_s \rangle + \langle N_c \rangle \langle \mathcal{N}_s \rangle^2)]. \quad (60)$$

This phenomenological model propagates the halo exclusion to galaxies, but it still does not correctly reproduce the stochasticity parameters measured from simulations: it over-predicts the super-Poissonian stochasticity by a factor of 10 and under-predicts the sub-Poissonian behavior. To compensate for the former, we multiply the answer by a fudge factor $g_{\alpha_0} = 0.072$. To account for the latter, we add the exclusion window contribution, which we weight over the HOD and correct by another fudge factor $g_{\text{excl}} = 0.2 [h\text{Mpc}^{-1}]^3$, resulting in

$$\alpha_0^g = g_{\alpha_0} \tilde{\alpha}_0^g - \frac{4\pi g_{\text{excl}}}{3\bar{n}_g} \int d\ln M \bar{n}_h r_{\text{vir}}^3(M) \langle N_g \rangle, \quad (61)$$

where $r_{\text{vir}} = (3M/(800\bar{\rho}_m))^{1/3}$. The resulting model reproduces the distribution of stochasticity EFT parameters quite well.

As far as the scale dependent stochasticity parameter is concerned, eq. (58) suggests the following phenomenological modification,

$$\tilde{\alpha}_1^g = \frac{1}{\bar{n}_g} \int d \ln M \bar{n} \alpha_1(M) [\langle N_c \rangle (1 + 3 \langle \mathcal{N}_s \rangle + \langle \mathcal{N}_s \rangle^2)]. \quad (62)$$

To partly account for the exclusion effects, we add a weighted contribution from the hard sphere halo model of [63] and introduce two additional fudge factors which we calibrate from simulations,

$$\alpha_1^g = g_{\tilde{\alpha}_1} \tilde{\alpha}_1^g + \frac{4\pi g_{\alpha_1}}{30\bar{n}_g} \int d \ln M \bar{n} r_{\text{vir}}^5(M) \langle N_g \rangle \quad (63)$$

In practice, we use

$$g_{\tilde{\alpha}_1} = 5, \quad g_{\alpha_1} = 2 [h\text{Mpc}^{-1}]^5. \quad (64)$$

We adopt the above model as a baseline in what follows.

Finally, the halo model can be used to compute the stochastic $k^2 \mu^2$ counterterm in redshift space. As suggested by our previous discussion on RSD counterterms, we split the total counterterm into two pieces: the one “inherited” from halos ($\alpha_2^g|_{\text{halo}}$), and the one generated by the velocity bias ($\alpha_2^g|_{\text{vel.}}$), for which we use expressions involving the velocity dispersion. The latter corresponds to the redshift-space modification of the one-halo term and it has been studied in detail in the literature. It has a structure very similar to that of the super-Poissonian shot noise [40, 73],

$$\alpha_2^g = -\frac{1}{2\bar{n}_g^2} \int d \ln M \bar{n} \Sigma_M^2 \langle N_c \rangle (2 \langle \mathcal{N}_s \rangle + 2 \langle \mathcal{N}_s \rangle^2), \quad (65)$$

where an additional factor of 2 in front of $\langle \mathcal{N}_s \rangle^2$ above appeared because both satellite densities inside the halo is smeared by the virial motion. The problem with the above expression is that it does not correctly capture the velocity bias of the centrals. One possible resolution of this issue is to add the smeared combination of the one-halo term and the shot noise contribution, resulting in the expression,

$$-\frac{1}{2\bar{n}_g^2} \int d \ln M \bar{n} \Sigma_M^2 \langle N_c \rangle (1 + 3 \langle \mathcal{N}_s \rangle + 2 \langle \mathcal{N}_s \rangle^2). \quad (66)$$

This expression is phenomenological, and thus we anticipate that it will require fudge factors. Applying the velocity bias to the satellites and the centrals in the above

expression, and introducing fudge factors $g_{\alpha_c}, g_{\alpha_s}$ we finally get

$$\alpha_2^g|_{\text{vel.}} = - \int d \ln M \bar{n} \Sigma_M^2 \langle N_c \rangle \times [g_{\alpha_c} \alpha_c^2 + g_{\alpha_s} \alpha_s^2 \langle \mathcal{N}_s \rangle (3 + \langle \mathcal{N}_s \rangle)]. \quad (67)$$

The final expression for α_2^g is obtained by adding the piece inherited from the halo centers of mass,

$$\alpha_2^g|_{\text{halo}} = \int d \ln M \bar{n} \alpha_2^h(\nu) \langle N_c \rangle [1 + \langle \mathcal{N}_s \rangle (3 + \langle \mathcal{N}_s \rangle)]. \quad (68)$$

Putting all together, we write down the final model

$$\alpha_2^g = g_{\alpha_2^h} \alpha_2^g|_{\text{halo}} + \alpha_2^g|_{\text{vel.}}, \quad (69)$$

where α_2^g is another fudge factor. A good match to data is obtained by setting

$$g_{\alpha_2^h} = 0.2, \quad g_{\alpha_c} = -1.5, \quad g_{\alpha_s} = 0.0033, \quad (70)$$

where the last two factors are given in units of $[h\text{Mpc}^{-1}]^2$. Comparing these fudge factors with the predictions of the naive halo model, we see that the numerical data actually prefers a strong positive contribution from the centrals due to their velocity dispersion, a somewhat weaker contribution from the halo centers of mass, and a noticeably weaker contributions from the satellites [12]. The fact that the 1-halo term overprotects the large and negative α_2^g , which contradicts the N-body data was previously pointed out by [73].

It is suggestive that the tension between the halo model predictions for the stochastic RSD counterterm could be resolved once the halo exclusion effects are taken into account. In addition, the positive sign of α_2 obtained in N-body simulations could be explained by the modulation of the galaxy power spectrum by the correlation function of virialized velocity fields inside the halo [73]. We defer a detailed analytic modeling of α_2 to future work, and use the phenomenological expression (69) in the rest of our paper.

3. COMPARISON WITH SIMULATIONS

In this section we compare our analytic predictions with the EFT parameter measurements from **AbacusSummit** simulations [83] carried out in [19, 21]. The caveat here is that these works produced EFT samples

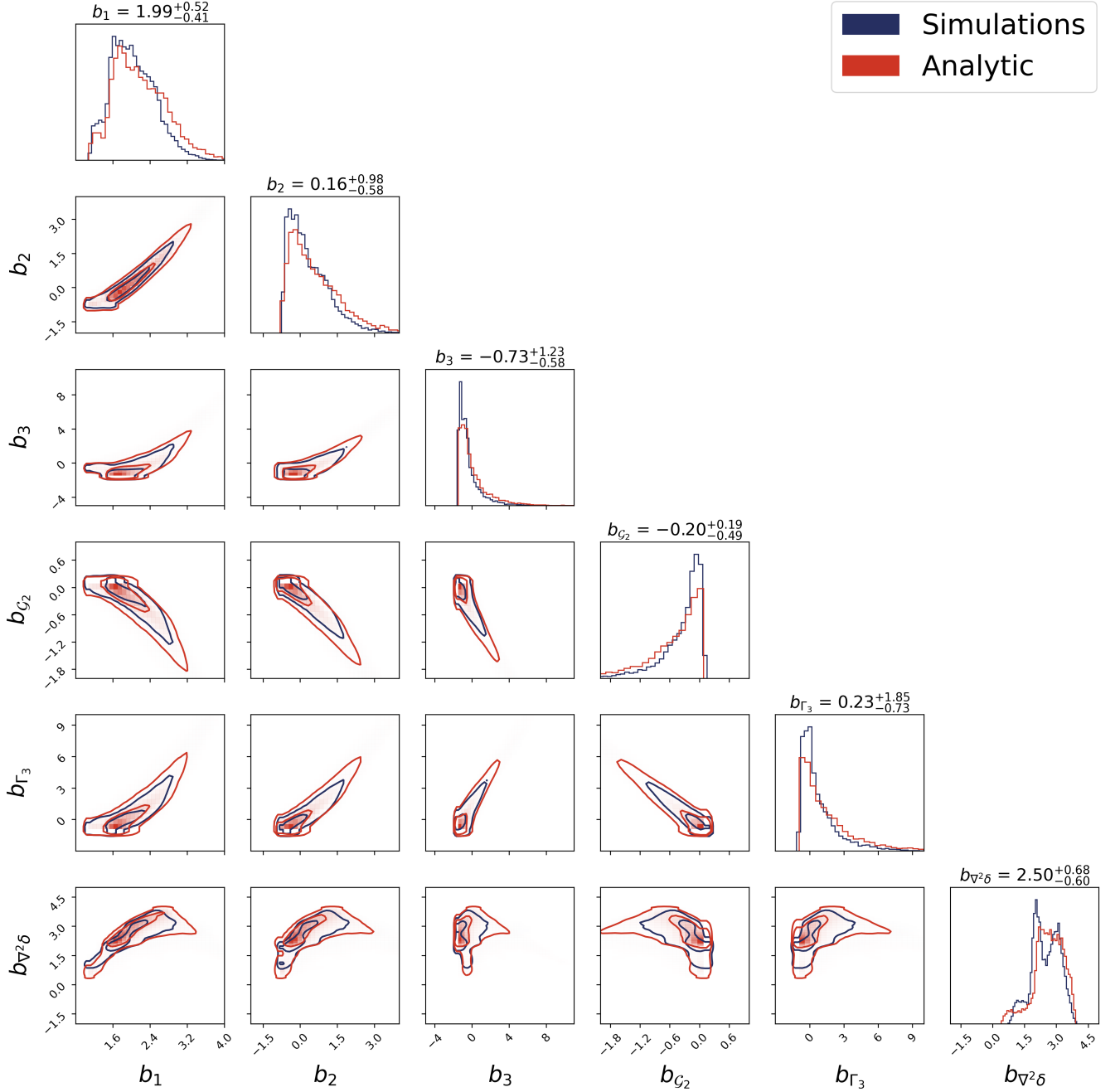


FIG. 3. The density of EFT galaxy bias parameters for HOD models extracted from N-body simulations (blue) and generated with our analytic model (red). Density levels correspond to two-dimensional 1- σ and 2- σ intervals (i.e. 39.3% and 86.5% of samples).

for decorated HODs. In order to produce the samples for the base HOD we use the EFT parameter distribution conditioned on the HOD parameters estimated by the normalizing flows following the approach of ref. [21].

We generate the samples of EFT parameters by numerically evaluating our analytical formulas for a large grid

of HOD parameters, which we randomly sample from the

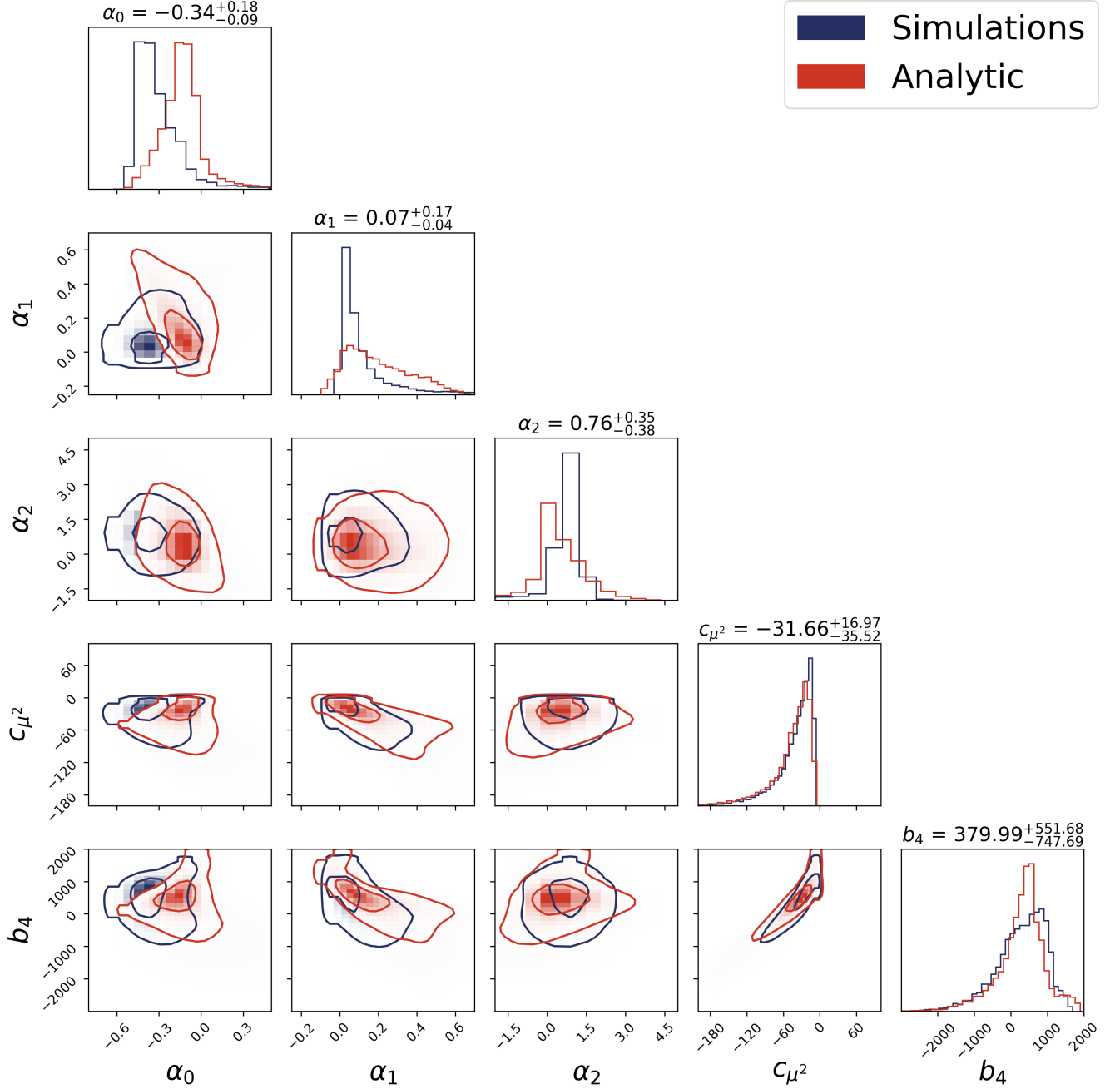


FIG. 4. Same as fig. 3 but for the stochastic EFT parameters and redshift-space counterterms.

following flat distribution from [21]:

$$\begin{aligned}
 \log_{10} M_{\text{cut}} &\in [12.4, 13.3], \quad \log_{10} M_1 \in [13.2, 14.4], \\
 \log_{10} \sigma &\in [-3.0, 0.0], \quad \alpha \in [0.7, 1.5], \quad \kappa \in [0.0, 1.5], \\
 \alpha_c &\in [0, 0.5], \quad \alpha_s \in [0.7, 1.3],
 \end{aligned}
 \tag{71}$$

where the halo masses are given in units of $h^{-1} M_{\odot}$. With a slight abuse of terminology, we will call the HOD priors

generated by numerically evaluating our analytic expressions “analytic priors,” even though there are no closed expressions for the EFT parameters that one can use.

Our results are presented in figs. 3 4 and in table I, where we show the mean values and standard deviations of the EFT parameters.

We start our comparison with the bias parameters. The density of our analytic HOD samples and the sam-

ples from the simulations for the same set of HOD parameters are displayed in fig. 3. Overall, our analytic model works for the bias parameters quite well, estimating the 1D marginal distributions within $\lesssim 40\%$. We find the largest discrepancy at the level of b_3 . However, since this parameter does not appear in the one-loop power spectrum model, it is irrelevant for actual data analyses based on the tree-level bispectrum e.g. [7, 84, 85].

The stochasticity parameters and RSD counterterms are presented in fig. 4. We observe highly consistent results for the redshift space counterterms. In particular, the 1D mean and standard deviations of b_4 and c_{μ^2} are reproduced to within 10%.

Importantly, our simple analytic model for the deterministic EFT parameters (bias parameters and RSD counterterms) reproduces all non-Gaussian correlations between them.

We find consistent results for the stochasticity EFT parameters $\alpha_0, \alpha_1, \alpha_2$, but the good agreement in this case is to a large extent thanks for fudge factors that we have calibrated to reproduce the target standard deviations of the HOD priors. Even with these additional fudge factors the agreement is typically within $\lesssim 40\%$. While this error is acceptable for the generation of EFT priors, it clearly calls for the development of more realistic models for the stochastic part of the galaxy power spectrum.

Param.	Analytic	Simulation
b_1	2.19 ± 0.56	2.05 ± 0.49
b_2	0.62 ± 1.02	0.37 ± 0.82
b_3	0.14 ± 1.65	-0.38 ± 1.21
$b_{\mathcal{G}_2}$	-0.56 ± 0.64	-0.46 ± 0.47
b_{Γ_3}	1.53 ± 2.42	1.14 ± 1.81
$b_{\nabla^2\delta}$	2.62 ± 0.68	2.19 ± 0.67
α_0	-0.12 ± 0.20	-0.29 ± 0.20
α_1	0.19 ± 0.17	0.14 ± 0.19
α_2	0.26 ± 1.53	0.51 ± 1.36
c_{μ^2}	-46.99 ± 34.93	-40.93 ± 31.40
b_4	290 ± 648	282 ± 686

TABLE I. Mean values and standard deviation of the EFT parameter samples from our analytic approach and simulations generated for the same range of HOD parameters for the *Planck2018* cosmology [86]. $b_{\nabla^2\delta}$ and c_{μ^2} are quoted in units $[h^{-1}\text{Mpc}]^2$, while for b_4 we use units of $[h^{-1}\text{Mpc}]^4$.

Note that the agreement between the simulations and the deterministic EFT parameters is a highly non-trivial test of our analytic approach, as well as the simulation-based field-level priors derived in [19, 21]. Indeed, if our field-level fits for the *halo* bias dependencies $b_{\mathcal{O}_a}^h(\nu)$ had been biased by two-loop corrections (which is equivalent to a wrong choice of k_{max}), we would have obtained biased analytic predictions for $b_{\mathcal{O}_a}^g$ that would not match the parameters measured from the simulations.⁷

All in all, we conclude that our analytic approach based on the halo model leads to an excellent agreement with the N-body data for galaxy bias parameters and counterterms, and satisfactory results for the stochastic EFT parameters.

4. TESTING COSMOLOGY AND HOD DEPENDENCE OF THE EFT PRIORS

Let us discuss now the cosmology and HOD dependence of the EFT priors.

4.1. Analytic study

Let us first discuss the cosmology dependence of the galaxy EFT parameters, following from the analytic equation (39). This will allow us to gain insights into the cosmology-dependence of EFT parameters at the qualitative level, and to some degree at the quantitative level.

Let us first discuss galaxy bias. It is useful to switch the integration variable in the HOD integrals from the mass to the peak height parameter ν , in which case the relevant integral takes the form

$$b_{\mathcal{O}_a}^g = \frac{1}{\bar{n}_g} \int d\nu \frac{d\bar{n}(\nu)}{d\nu} \langle N_g \rangle_M b_{\mathcal{O}_a}^h(\nu), \quad (72)$$

where $\frac{d\bar{n}(\nu)}{d\nu}$ is given by:

$$\frac{d\bar{n}(\nu)}{d\nu} = \frac{d\bar{n}}{d\ln M} \frac{d\ln M}{d\nu} = \frac{\bar{\rho}_m(t_0)}{M} f(\nu). \quad (73)$$

In order to obtain closed analytic expressions, let us assume a power-law cosmology. The linear matter power

⁷ Note that the two-loop corrections of halos and HOD galaxies are different, so if present, they would be expected to bias halo and HOD measurements differently.

spectrum is given by

$$P_{11}(k) = \frac{2\pi^2}{k_{\text{NL}}^3} \frac{k^n}{k_{\text{NL}}^n}, \quad (74)$$

where k_{NL} is the non-linear scale. By definition, it is the scales at which the position space density variance becomes of order unity, which is particularly easy to see from the above definition. Note that k_{NL} has a non-trivial redshift-dependence which can be inferred from the linear theory scaling $P_{11} \propto D_+^2(z)$. The peak height in the power law cosmology is given by

$$\nu = \delta_c \left(\frac{M}{\tilde{M}_{\text{NL}}} \right)^{\frac{n+3}{6}} \equiv \left(\frac{M}{M_{\text{NL}}} \right)^{\frac{n+3}{6}}, \quad (75)$$

$$M = M_{\text{NL}} \nu^{\frac{6}{n+3}},$$

where we used

$$\sigma_M^2(z) = (\tilde{M}_{\text{NL}}/M)^{\frac{n+3}{3}},$$

$$\tilde{M}_{\text{NL}} \equiv \left(\frac{9(1+n)\Gamma(n-1)\sin(\frac{\pi n}{2})}{2^n(n-3)} \right)^{\frac{3}{n+3}} \frac{4\pi\Omega_{m,0}\rho_c}{3k_{\text{NL}}^3(z)}, \quad (76)$$

and $4\pi R^3 \rho_c \Omega_{m,0}/3 = M$. This implies that⁸

$$b_{\mathcal{O}_a}^g = \frac{\int d\nu f(\nu) \nu^{-\frac{6}{n+3}} \langle N_g \rangle_{M[\nu]} b_{\mathcal{O}_a}^h(\nu)}{\int d\nu f(\nu) \nu^{-\frac{6}{n+3}} \langle N_g \rangle_{M[\nu]}}. \quad (77)$$

We observe that there are two sources of cosmology-dependence: the factor $\nu^{-\frac{6}{n+3}} \propto M^{-1}$ from the HMF and the HOD dependence of M whose mapping to ν is cosmology-dependent. Using the standard HOD parametrization (40), eq. (77) can be rewritten as

$$b_{\mathcal{O}_a}^g = \frac{1}{\mathcal{N}} \left(b_{\mathcal{O}_a}^g \Big|_c + b_{\mathcal{O}_a}^g \Big|_s \right), \quad (78)$$

where

$$b_{\mathcal{O}_a}^g \Big|_s = \int d\nu f(\nu) \nu^{-\frac{6}{n+3}} \langle N_c \rangle \left(\frac{\nu^{\frac{6}{n+3}} - \kappa \nu_{\text{cut}}^{\frac{6}{n+3}}}{\mathcal{M}_1} \right)^\alpha b_{\mathcal{O}_a}^h(\nu),$$

$$b_{\mathcal{O}_a}^g \Big|_c = \int d\nu f(\nu) \nu^{-\frac{6}{n+3}} \langle N_c \rangle_\nu b_{\mathcal{O}_a}^h(\nu), \quad (79)$$

and we introduced

$$\mathcal{N} = \int d\nu f(\nu) \nu^{-\frac{6}{n+3}} \langle N_g \rangle,$$

$$\langle N_c \rangle_\nu = \frac{1}{2} \left[1 + \text{Erf} \left(\frac{\log \nu - \log \nu_{\text{cut}}}{\sqrt{2}\sigma'} \right) \right], \quad (80)$$

$$\nu_{\text{cut}} = \frac{\delta_c}{\sigma_{M_{\text{cut}}}} = \left(\frac{M_{\text{cut}}}{M_{\text{NL}}} \right)^{\frac{3+n}{6}},$$

and $\mathcal{M}_1 = M_1/M_{\text{NL}}$, $\sigma' = 6\sigma/(n+3)$. We see that the bias parameters of galaxies depend on the cosmological parameter n , the parameters ν_{cut} , σ' , M'_1 which mix cosmological and HOD parameters, and the HOD parameters α and κ .

Let us first study the dependence of the HOD on the amplitude of the matter power spectrum at a redshift z , parameterized by $\sigma_8(z)$. Consider two cosmologies with different values of this parameter, $\sigma_8(z)$ and $\sigma'_8(z)$. Changing cosmology from $\sigma_8(z)$ to $\sigma'_8(z)$ is equivalent to the re-scaling of ν_{cut} and M'_1 as

$$\nu_{\text{cut}} \rightarrow \nu'_{\text{cut}} = \nu_{\text{cut}} \frac{\sigma_8(z)}{\sigma'_8(z)},$$

$$\mathcal{M}_1 \rightarrow \mathcal{M}'_1 = \mathcal{M}_1 \left(\frac{\sigma_8}{\sigma'_8} \right)^{\frac{6}{n+3}} \quad (81)$$

Note that σ' , α , κ do not change in this case. The shift of (81) due to σ_8 is equivalent to shifts in ν_{cut} and \mathcal{M}_1 due to the change of the threshold halo masses M_{cut} and M_1 . In other words, the cosmology dependence is degenerate with the values of the HOD parameters themselves. To see that, let us require the same HOD as a function of ν in both cosmologies. This implies that

$$\nu_{\text{cut}} = \nu'_{\text{cut}} \Rightarrow M'_{\text{cut}} = M_{\text{cut}} \left(\frac{\sigma'_8}{\sigma_8} \right)^{\frac{6}{n+3}},$$

$$\mathcal{M}'_1 = \mathcal{M}_1 \Rightarrow M_1 = M_1 \left(\frac{\sigma'_8}{\sigma_8} \right)^{\frac{6}{n+3}}. \quad (82)$$

Using $n = -2$, $\sigma'_8 = 0.7$, and $\sigma_8 = 0.8$ we find that

$$\log M'_{\text{cut}} - \log M_{\text{cut}} = \log M'_1 - \log M_1 \approx -0.3. \quad (83)$$

Hence, a 10% shift in the amplitude of the linear matter power spectrum at a given redshift can be fully compensated by a relatively small shift of the threshold halo masses. The sign of the difference also makes sense: in a cosmology with weaker matter fluctuations, one has to decrease the threshold halo mass in order to maintain the same abundance of galaxies.

⁸ Note that the critical density is cosmology-independent in the appropriate units, $\rho_c = 2.77 \cdot 10^{11} h^2 M_\odot \text{Mpc}^{-3}$.

Note that our argument about the degeneracy between the linear mass fluctuation amplitude and the HOD parameters is, in fact, exact: one can absorb the $\sigma_8(z)$ dependence of eqs. (79) into the HOD parameters completely. The transformations required for that are simply

$$\nu_{\text{cut}} \rightarrow \nu_{\text{cut}} \frac{\sigma'_8(z)}{\sigma_8(z)}, \quad \mathcal{M}_1 \rightarrow \mathcal{M}_1 \left(\frac{\sigma'_8}{\sigma_8} \right)^{\frac{6}{n+3}}. \quad (84)$$

In the general Λ CDM case the rightmost transformation above will require an inversion of the function $\sigma_M(z)$, which can be easily done numerically.

The situation becomes more complicated once we consider the dependence on the effective tilt of the matter power spectrum n . As we can see from eqs. (79), it is impossible to eliminate this dependence completely even in the simplified example of the power-law cosmology. Therefore, we expect some degree of residual cosmology dependence. Quantifying this is one of the goals of our work.

As far as the RSD counterterms are concerned, the part inherited from the halos exhibits the same dependence on cosmology as the bias parameters, and therefore our conclusion about the approximate cosmology dependence is true for them. The additional terms that depend on the velocity bias are cosmology-dependent as well, but their amplitude is fully degenerate with the velocity bias parameters, and therefore, this cosmology dependence can be absorbed exactly. Note, however, that the higher order bias $b_{\nabla^2\delta}$ and the RSD counterterm c_{μ^2} also depend on the dark matter counterterms which are cosmology-dependent. For instance,

$$b_{\nabla^2\delta} = b'_{\nabla^2\delta} - b_1 c_s, \quad (85)$$

where c_s is the cosmology-dependent speed of sound of dark matter. In principle, the cosmology dependence of c_s can be estimated using semi-analytic arguments along the lines of [87–90]. However, for the purpose of our work, it will be sufficient to use the naturalness arguments, according to which c_s should be of the order of the error that we make by evaluating all EFT integrals up to the infinite momenta. It implies the estimate

$$c_s \sim \frac{61 D_+^2(z)}{1260 \pi^2} \int_{k_{\text{NL}}}^{\infty} dq P_{11}(q), \quad (86)$$

where $k_{\text{NL}} \sim 0.5 \, h\text{Mpc}^{-1}$ at $z = 0.5$. A variation of the linear matter power spectrum by $\sim 10\%$ would only

lead to a similar $\sim 10\%$ variation of c_s . This parameter by itself is a small part of $b_{\nabla^2\delta}$ ($c_s(z = 0.5) \simeq 0.5 \, [h^{-1}\text{Mpc}]^2$), which changes by a factor of few under the variation of HOD parameters. Thus, we conclude that the cosmology-dependence of the dark matter counterterms can be safely ignored.

Finally, let us comment on the cosmology dependence of the stochastic EFT parameters. Using the HOD expressions (60) and (62), and repeating our arguments for the galaxy bias, we can conclude that the dependence on $\sigma_M(z)$ can be absorbed into the HOD parameters exactly, but the dependence on the matter power spectrum slope will remain.

Let us now present explicit numerical results that will quantify the residual cosmology dependence within our analytic model.

4.2. Numerical results

To obtain numerical results for different cosmologies, we prepare a latin hypercube of cosmological parameters $\omega_b, \omega_{\text{cdm}}, n_s, h$, and σ_8 . We sample these parameters randomly from the following flat distributions

$$\begin{aligned} \omega_{\text{cdm}} &\in [0.1, 0.132], \quad \omega_b \in [0.0220, 0.0228], \\ h &\in [0.65, 0.75], \quad n_s \in [0.9, 1.01], \quad \sigma_8 \in [0.6, 0.9]. \end{aligned} \quad (87)$$

We keep the total neutrino mass to be fixed to its minimally allowed value 0.06 eV. For parameters ω_{cdm} and n_s our priors correspond to approximately $10\times$ the width of the *Planck2018* standard deviations [86]. For ω_b we use only one standard deviation as this parameter is determined from the CMB in a nearly model-independent way. The wide ranges of h and σ_8 we use are motivated by the so-called H_0 and σ_8 tensions [91].

In the cosmology-dependent sample we use the same priors on the HOD parameters as we used before (71). To test the assertion that the cosmology-dependence is degenerate with the HOD parameters, we compare our cosmology dependent EFT parameters samples with those samples from HOD models at a fixed cosmology, but with wider priors on HOD parameters. To that end we use the following HOD priors motivated by [19, 92]:

$$\begin{aligned} \log_{10} M_{\text{cut}} &\in [12, 14], \quad \log_{10} M_1 \in [13, 15], \\ \log \sigma &\in [-3.5, 1.0], \quad \alpha \in [0.5, 1.5], \\ \alpha_c &\in [0, 1], \quad \alpha_s \in [0, 2], \quad \kappa \in [0.0, 1.5]. \end{aligned} \quad (88)$$

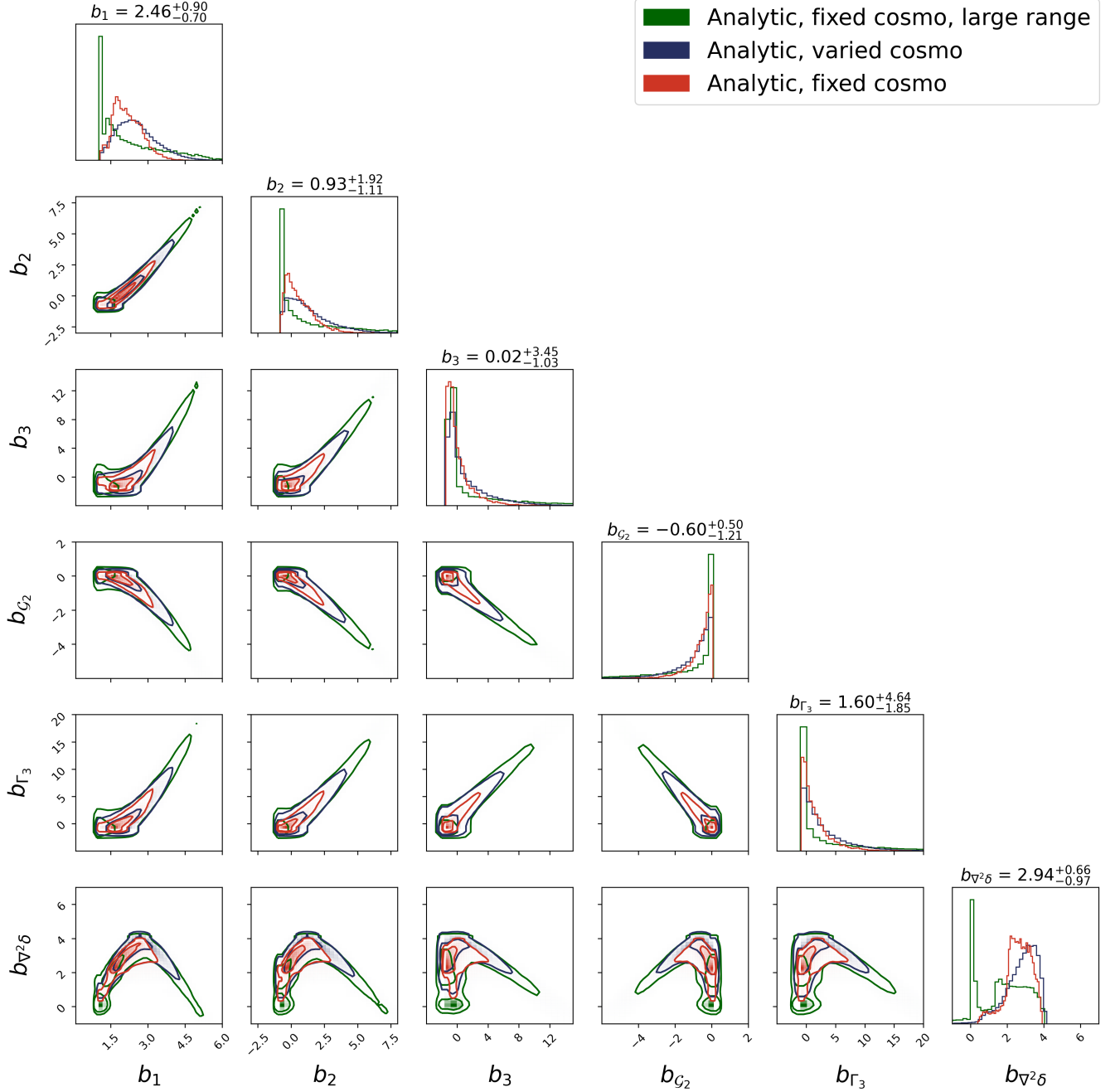


FIG. 5. The distribution of bias EFT parameters from our analytic model. We display the sample produced for a fixed cosmological model, and a wide range of the HOD parameters (green), the sample produced for the usual range of HOD parameters and by varying cosmology (blue), and the baseline sample produced at a fixed cosmology (red). Density levels correspond to two-dimensional 1σ and 2σ intervals (i.e. 39.3% and 86.5% of samples).

Our results are presented in figs. 5, 6 for the bias parameters and counterterms, respectively. For comparison, we also display the analytic samples at a fixed cosmology with the baseline HOD priors in this plot. The 1D intervals of the EFT parameter samples are presented

in table II. For comparison, we also quote the simulation results for the same HOD priors (88), as well as the simulation-based results from [19] for HOD models that include the decorated modifications. The corresponding distributions are displayed in figs. 7, 8.

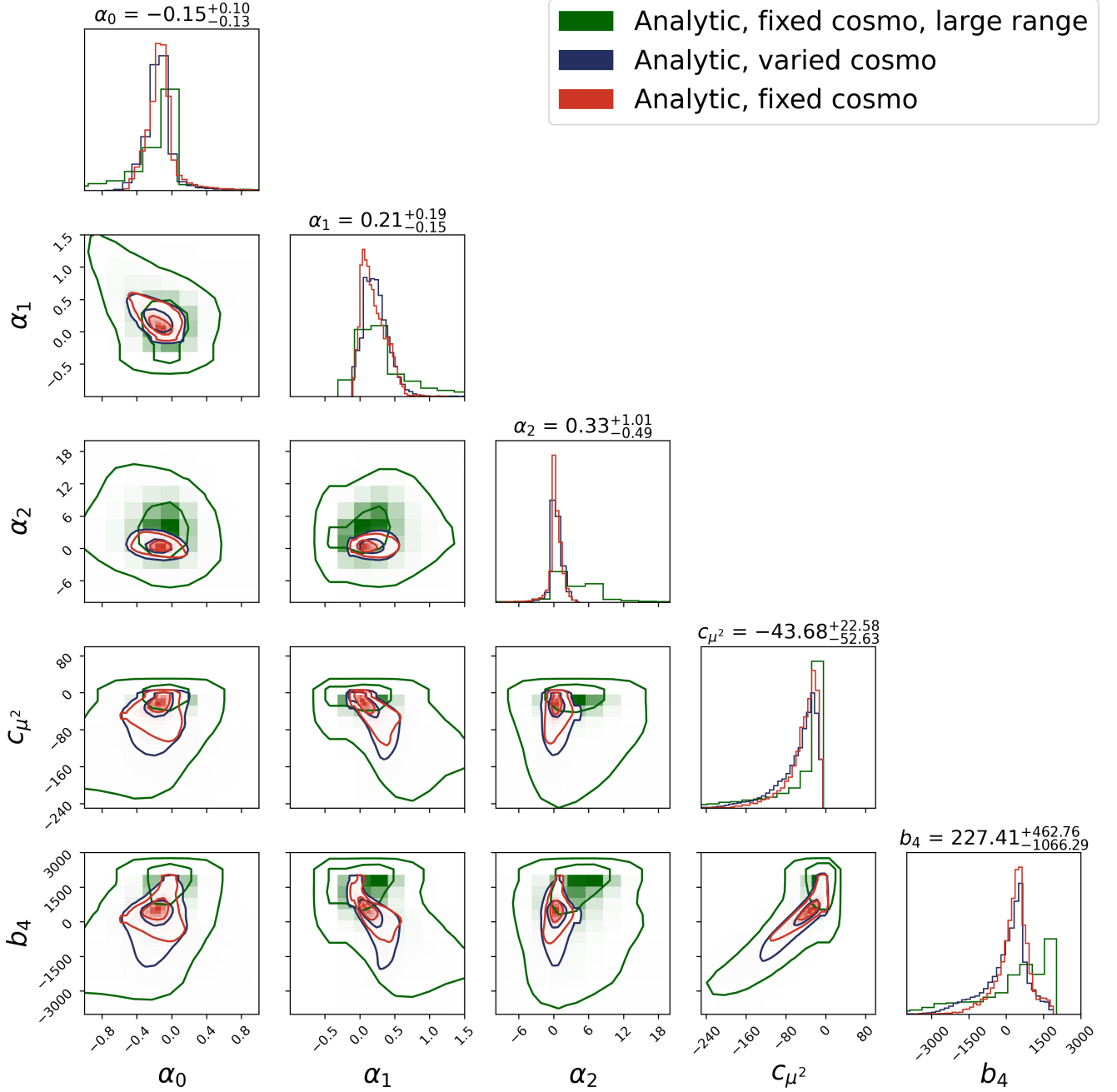


FIG. 6. Same as fig. 5 but for the stochastic EFT parameters and redshift-space counterterms.

Our results show that the variation of the HOD parameters produces a spread of the EFT parameters that is much wider than the one generated by the variation of cosmology. Comparing the fixed cosmology samples with the varied cosmology samples obtained under the same HOD priors, we note that the cosmology dependence only weakly affects the tails of the distribution, and therefore, at a leading order, it can be ignored altogether.

As a consistency check, we have compared our analytic results for EFT parameters of the base HOD models with wide priors with the simulations for the same HOD parameters. Overall, we find a good agreement, except for the $\alpha_{0,1}$ parameters, for which the width of the distribution appears to disagree with the simulations at about 100%. It is important to stress that our fudge factors for the stochastic parameters were calibrated to repro-

Param.	Fixed cosmo	Varied cosmo	Large range, fixed cosmo	Large range, Sim.	Decorated HOD (Sim.)
b_1	2.1898 ± 0.5624	2.5538 ± 0.7972	2.2778 ± 1.2808	2.1384 ± 1.1591	2.1260 ± 1.4268
b_2	0.6228 ± 1.0281	1.3060 ± 1.5831	1.1001 ± 2.5334	0.8188 ± 2.1090	0.8584 ± 2.1826
b_3	0.1388 ± 1.6579	1.1036 ± 2.8270	1.6913 ± 4.7106	1.0898 ± 4.0851	1.0881 ± 3.7282
$b_{\mathcal{G}_2}$	-0.5652 ± 0.6373	-0.9299 ± 1.0144	-0.9859 ± 1.7383	-0.8240 ± 1.4524	-0.9219 ± 2.0868
b_{Γ_3}	1.5299 ± 2.4241	2.9072 ± 3.8740	3.2070 ± 6.6383	2.6909 ± 5.7106	3.0875 ± 8.4037
$b_{\nabla^2\delta}$	2.6254 ± 0.6833	2.7869 ± 0.8382	1.6988 ± 1.3697	1.8742 ± 1.1757	1.2832 ± 6.3323
α_0	-0.1166 ± 0.2022	-0.1469 ± 0.1884	-0.1481 ± 0.4954	-0.0339 ± 0.8873	0.2653 ± 1.3830
α_1	0.1996 ± 0.1742	0.2293 ± 0.1795	0.3914 ± 0.5760	0.1275 ± 0.2743	0.0407 ± 0.2791
α_2	0.2585 ± 1.5363	0.3496 ± 1.4508	3.5524 ± 6.4653	-0.1371 ± 6.6088	-1.5075 ± 10.7245
c_{μ^2}	-46.9907 ± 34.9312	-57.4220 ± 44.0448	-72.2467 ± 111.7737	-65.4102 ± 101.8349	-65.1294 ± 100.2469
b_4	290.1989 ± 648.1431	8.8693 ± 886.7947	-62.0217 ± 2413.4284	-10.8034 ± 2000.4312	58.3832 ± 2029.0751

TABLE II. Mean and standard deviation of EFT parameter samples generated with our analytic approach assuming a fixed cosmology (first column), varied cosmology (second column), or a fixed cosmology and an extended range of the HOD parameters (third column). For comparison, we also show the simulation results for the same large range of the HOD parameters derived within the base HOD model (fourth column), and for the decorated HOD models that incorporate effects of assembly bias and baryonic feedback (fifth column).

duce the standard deviations of the HOD-based samples from the previous section, which were drawn from more narrow priors. The discrepancy at the level of $\alpha_{0,1}$ is another call for a more realistic model. We note, however, that the width of the α_2 parameter is reproduced quite well, which implies that our analytic model correctly captures the parametric dependence of α_2 on the base HOD parameters.

As a final remark, let us notice while our analytic model reproduces well the base HOD results, the EFT parameters from the base HOD models in general appear to be somewhat different than the EFT samples of the decorated HOD models, see figs. 7, 8. In particular, certain correlation between the bias parameters e.g. $b_2 - b_1$ have a different slope. In addition, the decorated HOD model in general produce a wider spread of the EFT parameters. This is especially so for the counterterm $b_{\nabla^2\delta}$. For the stochastic and redshift space counterterms, however, the decorated HOD samples are quite similar to the usual base HOD results. All in all, figs. 7, 8 display the obvious limitations of the base HOD framework, which is inherited in our analytic approach. This suggests that the use of the base HOD to generate the priors may lead to unrealistically narrow EFT priors, which will lead to biased estimates of cosmological parameters.

5. CONCLUSIONS

We have presented an analytic method to generate approximate simulation-based priors for the EFT-based full-shape analysis based on the halo model framework. Our method builds on three key ingredients: (a) a universal analytic model for the halo mass function, (b) the standard 7-parameter HOD parametrization, and (c) the assumption that the halo EFT parameters depend only on the peak height. In addition, we introduce a number of fudge parameters that account for the failure of the standard analytic halo model to account for the measured values of the stochastic EFT parameters.

While our analytic method is based on the above assumptions, which are quite restrictive, it offers many important practical advantages. First, it gives an analytic insight into the dependence of the EFT parameters on the HOD models and cosmology. In particular, we have proved analytically that the dependence of the EFT parameters on the amplitude of the linear matter power spectrum at a redshift of interest is completely degenerate with the threshold halo mass values. In a more general setting, our method allowed us to generate a sample of EFT parameters for a large grid of cosmological models and demonstrate explicitly that the cosmology-independence of the EFT parameters within the HOD

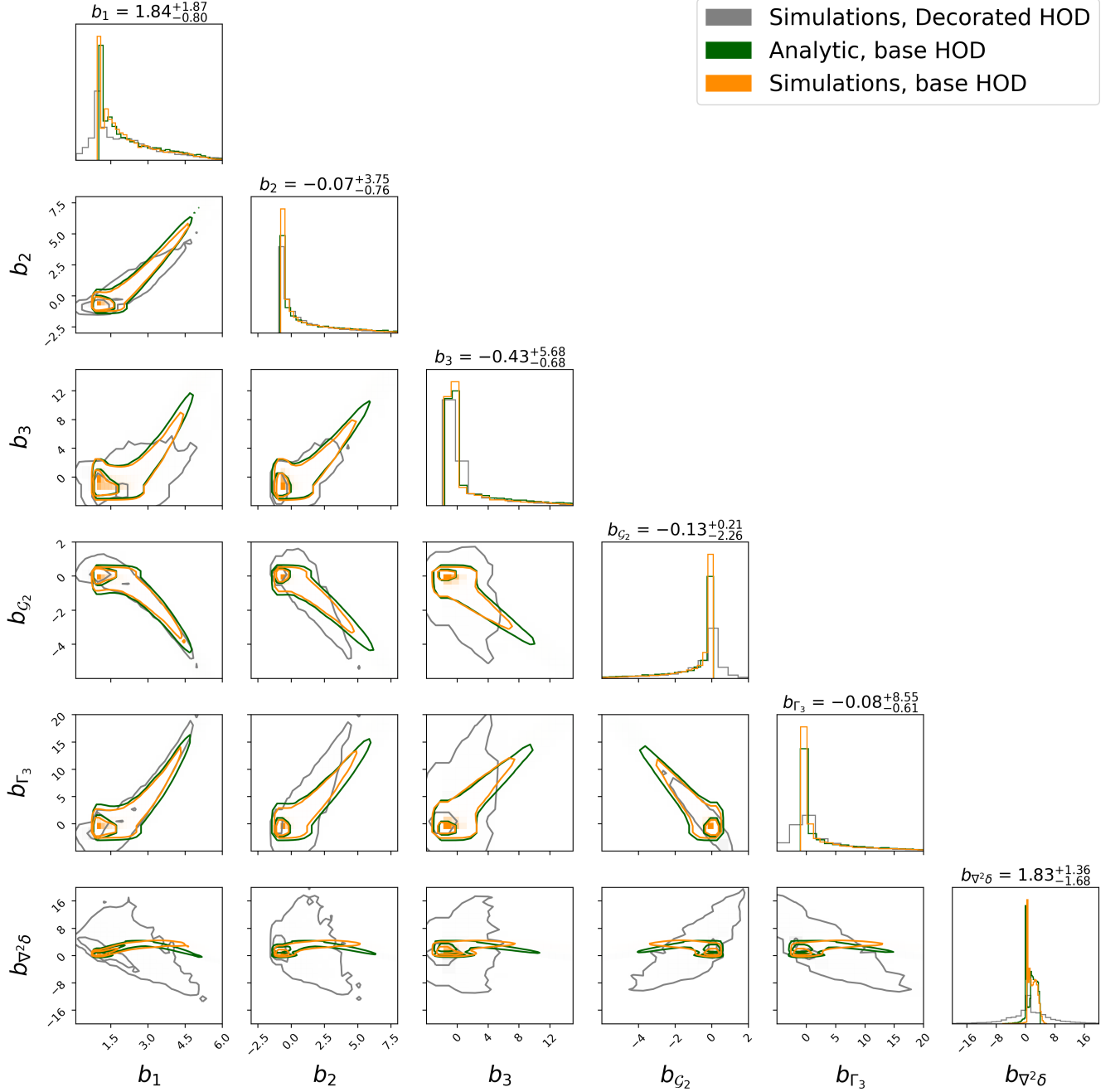


FIG. 7. The distribution of bias EFT parameters from our analytic model (dark green), the simulated base HOD catalogs (orange), and the simulated decorated HOD catalogs (gray).

models is negligible for the purpose of the prior generation.

A second important advantage of our approach is that it allows one to easily estimate the EFT parameters of galaxies at different redshifts. For instance, it can be used to get insight into the EFT parameters of quasars [93] or the high-redshift galaxies relevant for Spec-5 surveys [94].

An important application of our approach is the estimation of EFT parameters in extended cosmological models. For instance, our approach applies directly to models beyond Λ CDM that modify the shape of the linear matter power spectrum before recombination [95–99], or scenarios that only change the background expansion rate, such as a non-zero spatial curvature or dynamical

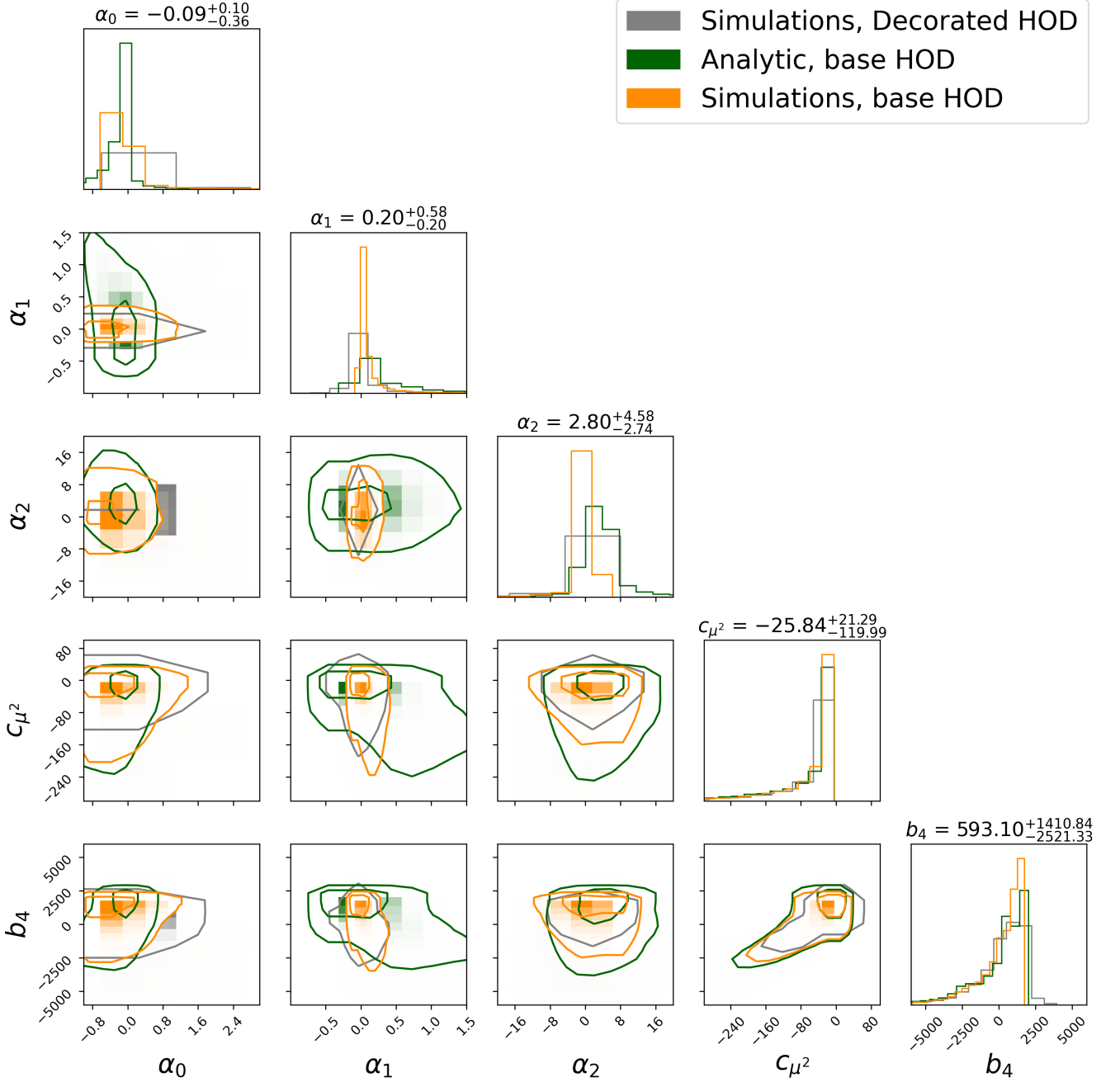


FIG. 8. Same as fig. 7 but for the stochastic EFT parameters and redshift-space counterterms.

dark energies [16]. In principle, our method can also be used to estimate EFT parameters in other extended cosmological models that modify the clustering at low redshifts, such as the ultralight axion dark matter [100] or massive light relics [101]. We caution, however, that some of the assumptions behind our approach, such as the universality of the halo mass mass function, may be violated in such models.

From the theory side, it will be important to develop a more realistic model for the stochastic EFT counterterms that incorporates the exclusion effects along the lines of [22, 63].

Finally, it will be interesting to apply our approach to other galaxy samples with different HOD parameterizations, e.g. emission line galaxies [38, 102] or quasars [93, 103]. We leave all the above research di-

rection for future work.

ACKNOWLEDGMENTS

We are grateful to Jamie Sullivan for useful conversations.

-
- [1] D. Baumann, A. Nicolis, L. Senatore, and M. Zaldarriaga, *JCAP* **1207**, 051 (2012), [arXiv:1004.2488 \[astro-ph.CO\]](#).
 - [2] J. J. M. Carrasco, M. P. Hertzberg, and L. Senatore, *JHEP* **09**, 082 (2012), [arXiv:1206.2926 \[astro-ph.CO\]](#).
 - [3] M. M. Ivanov, (2022), [arXiv:2212.08488 \[astro-ph.CO\]](#).
 - [4] M. M. Ivanov, M. Simonović, and M. Zaldarriaga, *JCAP* **05**, 042 (2020), [arXiv:1909.05277 \[astro-ph.CO\]](#).
 - [5] G. D’Amico, J. Gleyzes, N. Kokron, D. Markovic, L. Senatore, P. Zhang, F. Beutler, and H. Gil-Marín, (2019), [arXiv:1909.05271 \[astro-ph.CO\]](#).
 - [6] S.-F. Chen, Z. Vlah, and M. White, *JCAP* **02**, 008 (2022), [arXiv:2110.05530 \[astro-ph.CO\]](#).
 - [7] O. H. E. Philcox and M. M. Ivanov, *Phys. Rev. D* **105**, 043517 (2022), [arXiv:2112.04515 \[astro-ph.CO\]](#).
 - [8] S.-F. Chen, M. M. Ivanov, O. H. E. Philcox, and L. Wenzl, (2024), [arXiv:2406.13388 \[astro-ph.CO\]](#).
 - [9] A. G. Adame *et al.* (DESI), (2024), [arXiv:2411.12021 \[astro-ph.CO\]](#).
 - [10] S. Chen *et al.*, (2024), [arXiv:2407.04795 \[astro-ph.CO\]](#).
 - [11] M. M. Ivanov, *Phys. Rev. D* **109**, 023507 (2024), [arXiv:2309.10133 \[astro-ph.CO\]](#).
 - [12] M. M. Ivanov, M. W. Toomey, and N. G. Karaçaylı, (2024), [arXiv:2405.13208 \[astro-ph.CO\]](#).
 - [13] R. de Belsunce, S.-F. Chen, M. M. Ivanov, C. Ravoux, S. Chabanier, J. Sexton, and Z. Lukic, (2024), [arXiv:2412.06892 \[astro-ph.CO\]](#).
 - [14] D. Wadekar, M. M. Ivanov, and R. Scoccimarro, *Phys. Rev. D* **102**, 123521 (2020), [arXiv:2009.00622 \[astro-ph.CO\]](#).
 - [15] G. Cabass, M. M. Ivanov, O. H. E. Philcox, M. Simonovic, and M. Zaldarriaga, (2022), [arXiv:2211.14899 \[astro-ph.CO\]](#).
 - [16] A. Chudaykin, K. Dolgikh, and M. M. Ivanov, *Phys. Rev. D* **103**, 023507 (2021), [arXiv:2009.10106 \[astro-ph.CO\]](#).
 - [17] A. Chudaykin, M. M. Ivanov, and T. Nishimichi, (2024), [arXiv:2410.16358 \[astro-ph.CO\]](#).
 - [18] S. Paradiso, M. Bonici, M. Chen, W. J. Percival, G. D’Amico, H. Zhang, and G. McGee, (2024), [arXiv:2412.03503 \[astro-ph.CO\]](#).
 - [19] M. M. Ivanov, A. Obuljen, C. Cuesta-Lazaro, and M. W. Toomey, (2024), [arXiv:2409.10609 \[astro-ph.CO\]](#).
 - [20] G. Cabass, O. H. E. Philcox, M. M. Ivanov, K. Akitsu, S.-F. Chen, M. Simonović, and M. Zaldarriaga, (2024), [arXiv:2404.01894 \[astro-ph.CO\]](#).
 - [21] M. M. Ivanov, C. Cuesta-Lazaro, S. Mishra-Sharma, A. Obuljen, and M. W. Toomey, *Phys. Rev. D* **110**, 063538 (2024), [arXiv:2402.13310 \[astro-ph.CO\]](#).
 - [22] J. M. Sullivan, U. Seljak, and S. Singh, *JCAP* **11**, 026 (2021), [arXiv:2104.10676 \[astro-ph.CO\]](#).
 - [23] M. Zennaro, R. E. Angulo, S. Contreras, M. Pellejero-Ibáñez, and F. Maion, *Mon. Not. Roy. Astron. Soc.* **514**, 5443 (2022), [arXiv:2110.05408 \[astro-ph.CO\]](#).
 - [24] H. Zhang, M. Bonici, G. D’Amico, S. Paradiso, and W. J. Percival, (2024), [arXiv:2409.12937 \[astro-ph.CO\]](#).
 - [25] K. Akitsu, (2024), [arXiv:2410.08998 \[astro-ph.CO\]](#).
 - [26] M. Schmittfull, Z. Vlah, and P. McDonald, *Phys. Rev. D* **93**, 103528 (2016), [arXiv:1603.04405 \[astro-ph.CO\]](#).
 - [27] F. Schmidt, F. Elsner, J. Jasche, N. M. Nguyen, and G. Lavaux, *JCAP* **01**, 042 (2019), [arXiv:1808.02002 \[astro-ph.CO\]](#).
 - [28] F. Schmidt, (2020), [arXiv:2012.09837 \[astro-ph.CO\]](#).
 - [29] F. Schmidt, (2020), [arXiv:2009.14176 \[astro-ph.CO\]](#).
 - [30] F. Schmidt, G. Cabass, J. Jasche, and G. Lavaux, *JCAP* **11**, 008 (2020), [arXiv:2004.06707 \[astro-ph.CO\]](#).
 - [31] N.-M. Nguyen, F. Schmidt, B. Tucci, M. Reinecke, and A. Kostić, (2024), [arXiv:2403.03220 \[astro-ph.CO\]](#).
 - [32] M. M. Abidi and T. Baldauf, *JCAP* **1807**, 029 (2018), [arXiv:1802.07622 \[astro-ph.CO\]](#).
 - [33] M. Schmittfull, M. Simonović, V. Assassi, and M. Zaldarriaga, *Phys. Rev. D* **100**, 043514 (2019), [arXiv:1811.10640 \[astro-ph.CO\]](#).
 - [34] M. Schmittfull, M. Simonović, M. M. Ivanov, O. H. E. Philcox, and M. Zaldarriaga, *JCAP* **05**, 059 (2021), [arXiv:2012.03334 \[astro-ph.CO\]](#).
 - [35] A. A. Berlind, D. H. Weinberg, A. J. Benson, C. M. Baugh, S. Cole, R. Dave, C. S. Frenk, A. Jenkins, N. Katz, and C. G. Lacey, *Astrophys. J.* **593**, 1 (2003), [arXiv:astro-ph/0212357](#).

- [36] Z. Zheng, A. A. Berlind, D. H. Weinberg, A. J. Benson, C. M. Baugh, S. Cole, R. Dave, C. S. Frenk, N. Katz, and C. G. Lacey, *Astrophys. J.* **633**, 791 (2005), [arXiv:astro-ph/0408564](#).
- [37] R. H. Wechsler and J. L. Tinker, *Ann. Rev. Astron. Astrophys.* **56**, 435 (2018), [arXiv:1804.03097 \[astro-ph.GA\]](#).
- [38] M. M. Ivanov *et al.*, (2024), [arXiv:2412.01888 \[astro-ph.CO\]](#).
- [39] U. Seljak, *Mon. Not. Roy. Astron. Soc.* **318**, 203 (2000), [arXiv:astro-ph/0001493](#).
- [40] U. Seljak, *Mon. Not. Roy. Astron. Soc.* **325**, 1359 (2001), [arXiv:astro-ph/0009016](#).
- [41] A. Cooray and R. K. Sheth, *Phys. Rept.* **372**, 1 (2002), [arXiv:astro-ph/0206508](#).
- [42] A. J. Benson, S. Cole, C. S. Frenk, C. M. Baugh, and C. G. Lacey, *Mon. Not. Roy. Astron. Soc.* **311**, 793 (2000), [arXiv:astro-ph/9903343](#).
- [43] V. Desjacques, D. Jeong, and F. Schmidt, *Phys. Rept.* **733**, 1 (2018), [arXiv:1611.09787 \[astro-ph.CO\]](#).
- [44] W. H. Press and P. Schechter, *Astrophys. J.* **187**, 425 (1974).
- [45] R. K. Sheth and G. Tormen, *Mon. Not. Roy. Astron. Soc.* **308**, 119 (1999), [arXiv:astro-ph/9901122](#).
- [46] J. L. Tinker, A. V. Kravtsov, A. Klypin, K. Abazajian, M. S. Warren, G. Yepes, S. Gottlober, and D. E. Holz, *Astrophys. J.* **688**, 709 (2008), [arXiv:0803.2706 \[astro-ph\]](#).
- [47] Y. Li and R. E. Smith, (2024), [arXiv:2411.18722 \[astro-ph.CO\]](#).
- [48] A. P. Hearin, A. R. Zentner, F. C. van den Bosch, D. Campbell, and E. Tollerud, *Mon. Not. Roy. Astron. Soc.* **460**, 2552 (2016), [arXiv:1512.03050 \[astro-ph.CO\]](#).
- [49] T. Lazeyras, A. Barreira, and F. Schmidt, *JCAP* **10**, 063 (2021), [arXiv:2106.14713 \[astro-ph.CO\]](#).
- [50] L. Lucie-Smith, A. Barreira, and F. Schmidt, *Mon. Not. Roy. Astron. Soc.* **524**, 1746 (2023), [arXiv:2304.09880 \[astro-ph.CO\]](#).
- [51] A. Chudaykin, M. M. Ivanov, O. H. E. Philcox, and M. Simonović, *Phys. Rev. D* **102**, 063533 (2020), [arXiv:2004.10607 \[astro-ph.CO\]](#).
- [52] S.-F. Chen, Z. Vlah, E. Castorina, and M. White, *JCAP* **03**, 100 (2021), [arXiv:2012.04636 \[astro-ph.CO\]](#).
- [53] M. M. Ivanov, A. A. Kaurov, and S. Sibiryakov, *JCAP* **1903**, 009 (2019), [arXiv:1811.07913 \[astro-ph.CO\]](#).
- [54] U. Seljak, A. Slosar, and P. McDonald, *JCAP* **10**, 014 (2006), [arXiv:astro-ph/0604335](#).
- [55] T. Kitayama and Y. Suto, *Astrophys. J.* **469**, 480 (1996), [arXiv:astro-ph/9604141](#).
- [56] V. Assassi, D. Baumann, D. Green, and M. Zaldarriaga, *JCAP* **1408**, 056 (2014), [arXiv:1402.5916 \[astro-ph.CO\]](#).
- [57] F. Bernardeau, S. Colombi, E. Gaztanaga, and R. Scoccimarro, *Phys. Rept.* **367**, 1 (2002), [arXiv:astro-ph/0112551 \[astro-ph\]](#).
- [58] M. White, *Mon. Not. Roy. Astron. Soc.* **439**, 3630 (2014), [arXiv:1401.5466 \[astro-ph.CO\]](#).
- [59] J. L. Tinker, B. E. Robertson, A. V. Kravtsov, A. Klypin, M. S. Warren, G. Yepes, and S. Gottlober, *Astrophys. J.* **724**, 878 (2010), [arXiv:1001.3162 \[astro-ph.CO\]](#).
- [60] A. Eggemeier, R. Scoccimarro, R. E. Smith, M. Crocce, A. Pezzotta, and A. G. Sánchez, (2021), [arXiv:2102.06902 \[astro-ph.CO\]](#).
- [61] T. Lazeyras, C. Wagner, T. Baldauf, and F. Schmidt, *JCAP* **1602**, 018 (2016), [arXiv:1511.01096 \[astro-ph.CO\]](#).
- [62] B. Hadzhiyska, D. Eisenstein, S. Bose, L. H. Garrison, and N. Maksimova, *Mon. Not. Roy. Astron. Soc.* **509**, 501 (2021), [arXiv:2110.11408 \[astro-ph.CO\]](#).
- [63] T. Baldauf, U. Seljak, R. E. Smith, N. Hamaus, and V. Desjacques, *Phys. Rev. D* **88**, 083507 (2013), [arXiv:1305.2917 \[astro-ph.CO\]](#).
- [64] A. Chudaykin, M. M. Ivanov, and M. Simonović, *Phys. Rev. D* **103**, 043525 (2021), [arXiv:2009.10724 \[astro-ph.CO\]](#).
- [65] L. Senatore and M. Zaldarriaga, (2014), [arXiv:1409.1225 \[astro-ph.CO\]](#).
- [66] A. Perko, L. Senatore, E. Jennings, and R. H. Wechsler, (2016), [arXiv:1610.09321 \[astro-ph.CO\]](#).
- [67] J. C. Jackson, *Mon. Not. Roy. Astron. Soc.* **156**, 1P (1972), [arXiv:0810.3908 \[astro-ph\]](#).
- [68] M. M. Ivanov, O. H. E. Philcox, M. Simonović, M. Zaldarriaga, T. Nischimichi, and M. Takada, *Phys. Rev. D* **105**, 043531 (2022), [arXiv:2110.00006 \[astro-ph.CO\]](#).
- [69] C. Cuesta-Lazaro *et al.*, (2023), [arXiv:2309.16539 \[astro-ph.CO\]](#).
- [70] C. Hahn, M. Eickenberg, S. Ho, J. Hou, P. Lemos, E. Massara, C. Modi, A. Moradinezhad Dizgah, L. Parker, and B. R.-S. Blancard, (2023), [arXiv:2310.15243 \[astro-ph.CO\]](#).
- [71] C. Hahn, M. Eickenberg, S. Ho, J. Hou, P. Lemos, E. Massara, C. Modi, A. Moradinezhad Dizgah, L. Parker, and B. R.-S. Blancard (SimBIG), *Phys. Rev. D* **109**, 083534 (2024), [arXiv:2310.15243 \[astro-ph.CO\]](#).
- [72] C. Hahn *et al.*, (2023), [arXiv:2310.15246 \[astro-ph.CO\]](#).
- [73] M. Maus *et al.*, (2024), [arXiv:2404.07312 \[astro-ph.CO\]](#).
- [74] M. J. White, *Mon. Not. Roy. Astron. Soc.* **321**, 1 (2001), [arXiv:astro-ph/0005085](#).
- [75] A. A. Berlind and D. H. Weinberg, *Astrophys. J.* **575**, 587 (2002), [arXiv:astro-ph/0109001](#).

- [76] N. Hand, U. Seljak, F. Beutler, and Z. Vlah, *JCAP* **1710**, 009 (2017), [arXiv:1706.02362 \[astro-ph.CO\]](#).
- [77] R. Scoccimarro, *Phys. Rev. D* **70**, 083007 (2004), [arXiv:astro-ph/0407214 \[astro-ph\]](#).
- [78] J. Hou *et al.* (eBOSS), *Mon. Not. Roy. Astron. Soc.* **480**, 2521 (2018), [arXiv:1801.02656 \[astro-ph.CO\]](#).
- [79] A. Eggemeier, N. Lee, R. Scoccimarro, B. Camacho-Quevedo, A. Pezzotta, M. Crocce, and A. G. Sánchez, (2025), [arXiv:2501.18597 \[astro-ph.CO\]](#).
- [80] M. M. Ivanov, (2021), [arXiv:2106.12580 \[astro-ph.CO\]](#).
- [81] A. Baleato Lizancos, U. Seljak, M. Karamanis, M. Bonici, and S. Ferraro, (2025), [arXiv:2501.10587 \[astro-ph.CO\]](#).
- [82] L. R. Abramo, I. Balmès, F. Lacasa, and M. Lima, *Mon. Not. Roy. Astron. Soc.* **454**, 2844 (2015), [arXiv:1506.02315 \[astro-ph.CO\]](#).
- [83] N. A. Maksimova, L. H. Garrison, D. J. Eisenstein, B. Hadzhiyska, S. Bose, and T. P. Satterthwaite, *Mon. Not. Roy. Astron. Soc.* **508**, 4017 (2021), [arXiv:2110.11398 \[astro-ph.CO\]](#).
- [84] M. M. Ivanov, O. H. E. Philcox, G. Cabass, T. Nishimichi, M. Simonović, and M. Zaldarriaga, *Phys. Rev. D* **107**, 083515 (2023), [arXiv:2302.04414 \[astro-ph.CO\]](#).
- [85] M. M. Ivanov, O. H. E. Philcox, T. Nishimichi, M. Simonović, M. Takada, and M. Zaldarriaga, *Phys. Rev. D* **105**, 063512 (2022), [arXiv:2110.10161 \[astro-ph.CO\]](#).
- [86] Planck Collaboration, N. Aghanim, and A. Zonca, *A&A* **641**, A6 (2020), [arXiv:1807.06209 \[astro-ph.CO\]](#).
- [87] A. Chudaykin, M. M. Ivanov, and S. Sibiryakov, *JCAP* **08**, 079 (2023), [arXiv:2212.09799 \[astro-ph.CO\]](#).
- [88] C. Nascimento, D. Jamieson, M. McQuinn, and M. Loverde, *JCAP* **02**, 023 (2025), [arXiv:2410.11949 \[astro-ph.CO\]](#).
- [89] T. Baldauf, E. Schaan, and M. Zaldarriaga, *JCAP* **03**, 017 (2016), [arXiv:1505.07098 \[astro-ph.CO\]](#).
- [90] T. Baldauf, E. Schaan, and M. Zaldarriaga, *JCAP* **03**, 007 (2016), [arXiv:1507.02255 \[astro-ph.CO\]](#).
- [91] E. Abdalla *et al.*, *JHEAp* **34**, 49 (2022), [arXiv:2203.06142 \[astro-ph.CO\]](#).
- [92] S. Yuan *et al.* (DESI), (2023), [arXiv:2310.09329 \[astro-ph.CO\]](#).
- [93] A. Chudaykin and M. M. Ivanov, (2022), [arXiv:2210.17044 \[astro-ph.CO\]](#).
- [94] J. Ravi, B. Hadzhiyska, M. J. White, L. Hernquist, and S. Bose, *Phys. Rev. D* **110**, 103509 (2024), [arXiv:2403.02414 \[astro-ph.CO\]](#).
- [95] A. He, M. M. Ivanov, R. An, and V. Gluscevic, *Astrophys. J. Lett.* **954**, L8 (2023), [arXiv:2301.08260 \[astro-ph.CO\]](#).
- [96] D. Camarena, F.-Y. Cyr-Racine, and J. Houghteling, *Phys. Rev. D* **108**, 103535 (2023), [arXiv:2309.03941 \[astro-ph.CO\]](#).
- [97] A. He, R. An, M. M. Ivanov, and V. Gluscevic, *Phys. Rev. D* **109**, 103527 (2024), [arXiv:2309.03956 \[astro-ph.CO\]](#).
- [98] A. He, M. M. Ivanov, R. An, T. Driskell, and V. Gluscevic, (2025), [arXiv:2502.02636 \[astro-ph.CO\]](#).
- [99] M. M. Ivanov, E. McDonough, J. C. Hill, M. Simonović, M. W. Toomey, S. Alexander, and M. Zaldarriaga, *Phys. Rev. D* **102**, 103502 (2020), [arXiv:2006.11235 \[astro-ph.CO\]](#).
- [100] K. K. Rogers, R. Hložek, A. Laguë, M. M. Ivanov, O. H. E. Philcox, G. Cabass, K. Akitsu, and D. J. E. Marsh, *JCAP* **06**, 023 (2023), [arXiv:2301.08361 \[astro-ph.CO\]](#).
- [101] W. L. Xu, J. B. Muñoz, and C. Dvorkin, *Phys. Rev. D* **105**, 095029 (2022), [arXiv:2107.09664 \[astro-ph.CO\]](#).
- [102] S. Alam, J. A. Peacock, K. Kraljic, A. J. Ross, and J. Comparat (eBOSS), *Mon. Not. Roy. Astron. Soc.* **497**, 581 (2020), [arXiv:1910.05095 \[astro-ph.CO\]](#).
- [103] A. Smith *et al.* (eBOSS), *Mon. Not. Roy. Astron. Soc.* **499**, 269 (2020), [arXiv:2007.09003 \[astro-ph.CO\]](#).